SIMULATED DYNAMICS OF THE AALC JEFF (B) CRAFT OVER WAVES

C.W. Lin

ORI, INC., Silver Spring, Maryland, USA

E. Zarnick and D.D. Moran

David W. Taylor Naval Ship Research and Development Center

Bethesda, Maryland, USA

ABSTRACT

A digital simulation to model the dynamics of an air-cushion-supported vehicle in operation over compliant waves has been developed. In the present investigation heave, pitch and roll motions of the JEFF (B) Amphibious Assault Landing Craft are predicted and compared with 1/12th model scale data (Ref. 1).

The JEFF (B) craft is a bag and finger type air cushion vehicle with longitudinal and transverse stability keels. The craft is assumed to be moving at constant speed and heading angle over a regular compliant wave. The compliance (free surface deformation) is computed by assuming a spatially varying pressure distribution under the craft. This spatial variation, which consists of combinations of linear and hyperbolic tangent segments, directly affects the cushion air flow computations. Specifically, the cushion volume variations due to craft orientation with respect to the free surface (craft pumping and wave pumping), and the escape area variations at the skirt/free surface interface critically depend on the nature of the free surface deformation resulting from the pressure distribution.

Hydrodynamic parameters which incorporate both spatial and speed dependency are obtained by a method based on Lamb's classical theory (Ref. 2). At each simulated time step the free surface deformation is evaluated by using these hydrodynamic parameters and corresponding cushion pressures generated in the previous time step. The non-linear air flow continuity equations are then solved to obtain the current cushion pressures. Newtonian equations of motion are thus formulated, and corresponding dynamic responses are obtained via a fourth order Runge-Kutta numerical procedure.

Computer generated time histories of heave, pitch and roll responses at constant surge speeds are transformed to the frequency domain by the FFT (Fast Fourier Transform) method to obtain transfer functions (Response Amplitude Operators, RAO). Several headings (i.e. head, following, beam and beam quartering seas) are investigated. The simulated results are found to be in reasonable agreement with experimental data for the 1/12th scale model JEFF (B) craft.

References:

(1) Kallio, J.A., "Results of Oblique Sea Experiments on the 1/12 Scale JEFF (B) Amphibious Assault Landing Craft," DTNSRDC, SPD-0859-01, September 1979.

(2) Lamb, H., Hydrodynamics, 6th Ed., Dover Publications, 1932, pp. 398-406.

APPLICATION OF SYSTEM IDENTIFICATION FLIGHT ANALYSIS TECHNIQUES TO THE PITCH-HEAVE DYNAMICS OF AN AIR CUSHION VEHICLE

P. A. Sullivan, F.C.A.S.I., P. V. Hartmann* and T. A. Graham

Institute for Aerospace Studies
University of Toronto
Toronto, Canada

ABSTRACT

This paper describes the analysis of flight test data obtained from the UTIAS Circular Track Test Vehicle, Vampire 1, which has base dimensions of 4.08m × 2.06m, and mass up to 850 kg. The skirt used for these tests was of the uncompartmented segmented skirt type, and the segment material was an 0.48 mm thick neoprene coated nylon fabric having a surface density of 0.54 kg/m^2, corresponding to about 0.6% of the equilibrium cushion pressure. The test data, consisting of outputs from accelerometers, angular rate gyros, and other instrumentation was obtained by flying the vehicle over a ramp installed in the 43m diameter track. It was analysed using a maximum likelihood, Gauss-Newton system identification (SPI) technique developed for the interpretation of flight test data of aircraft. The analysis assumed that the vehicle dynamics could be mathematically modelled by a linear fifth order system in the usual form $\dot{\underset{\sim}{x}} = \underset{\sim}{A}\,\underset{\sim}{x}$, corresponding to two orders each for the rigid body pitch and heave dynamics, and a fifth for the pneumatic capacitance of the cushion volume. However, since experimentally measured static pitch stiffness curves for this skirt material showed substantial hysteresis, additional equivalent linear dashpot damping terms were included in the formulation. The aim of the identification technique was to estimate values of the coefficients in the 5×5 $\underset{\sim}{A}$ matrix which allowed the mathematical model to best fit the data. The results were then compared with those that could be measured in the static experiments. Reasonable agreement was obtained between the estimates of stiffness and damping in pitch, and the corresponding values measured in the static pitch tests. This is a basic test of the effectiveness of the method. It also confirms that the hysteresis observed in the static pitch tests can have a major effect on the dynamics of the vehicle. The significance of this finding for full scale vehicle dynamics remains to be assessed.

INTRODUCTION

One of the air cushion technology research facilities at the Institute for Aerospace Studies of the University of Toronto (UTIAS), built with the aid of a Negotiated Grant from the National Research Council of Canada (NRC) in the early 1970's, is a large enclosed circular test track. This track, which is 43.6 metres in diameter, is intended for the investigation of the dynamics of a complete air cushion vehicle (ACV), and can test models having planform dimensions up to 4.08m × 2.06m and weighing as much as 8300 N (850 kg). The large size was chosen for two reasons: it enables the use of a sophisticated dynamics instrumentation package, and it aids the task of scaling the flexible materials used in the cushion systems of all modern ACV's.

The test vehicle, Vampire 1, shown in Fig. 1, is constrained to move in a circle on the track by a tether cable attached to a centre post. This tether cable also carries the vehicle control and data signal cables. The vehicle has separate lift and propulsion engines, each with its own throttle, and it is operated from a control room which overlooks the track. In normal operation, the vehicle is accelerated while resting on its wheels to a speed sufficient to keep the tether cable taut, and then the lift engine throttle is opened to inflate the cushion and thereby achieve lift-off. The track also has two hydraulically operated ramps located side by side and overlooked by the control room. They can be operated independently in order to induce either pitch or roll disturbances in the vehicle. Figure 1 shows the vehicle flying over the ramps when they are set for a pitch disturbance.

Currently Vampire 1 is equipped with three accelerometers and three rate gyros located at its centre of mass, a cushion pressure transducer, and three trailing arm sensors (TAS), one of which can be seen in Fig. 1. Rotary potentiometers are attached to the pivot of each TAS, so that vehicle motion generates time varying voltages from these potentiometers, which in turn can be interpreted to obtain direct information about the vehicle's instantaneous heave height and pitch and roll attitude. During the motion of the vehicle that occurs in response to a control or initial disturbance input, the response in time or histories of the electrical outputs of all of the transducers and some ancilliary information are recorded by a specially designed digital data acquisition system (DDAS) based on Intel 8080 and 6800 microprocessors. The DDAS has a master unit in the control room, which commands and controls a slave unit on the vehicle through a communication link

*Presently at de Havilland Aircraft of Canada, Toronto.

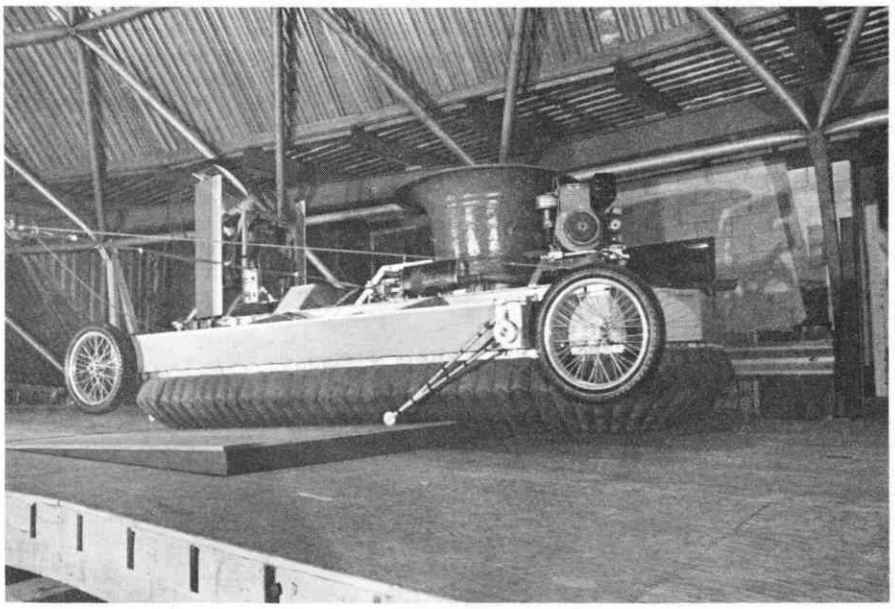


Fig. 1 Photograph of the UTIAS 43 metre Circular Track Test Vehicle, Vampire 1, in flight and traversing the ramps. The vehicle is equipped with an uncompartmented segmented skirt cushion, and the right front trailing arm is about to leave the ramp.

attached to the tether cable. In the slave unit, every 1/100 second, at a command from a crystal clock, the data is simultaneously sampled on all channels by sample-and-hold amplifiers. Then, one at a time, each sample is digitized and encoded for transmission along the communication link to the master unit. The data is then stored on magnetic tape by a Hewlett Packard HP2100 computer for subsequent analysis on the University's IBM 360 computer. The microprocessor also permits signal channel gains and offsets to be changed in the course of an experiment.[1]

The main objective of the UTIAS programme is the development of mathematical models of the dynamics of various flexible skirted cushion systems which can be used as aids to design. Initial Circular Track experiments focussed on specific cushion systems.[2,3] However, it was generally found that, while these investigations revealed some intriguing problems, they were in large part unsatisfactory, owing to the complexity of the skirt geometries, which introduced large nonlinearities, and to perceived skirt material scaling problems. However, they led to the definition of certain simpler projects, some of which have since been successfully completed. These projects have investigated such aspects of the complete cushion dynamics problem as the effect of ducting,[4,5] and viscoelastic properties of skirt materials on dynamic stability.[6] Hence the overall objective of our current Track project has now become the assessment of the accuracy with which our mathematical models, postulated with the aid of insights obtained from these simpler projects, can describe the dynamics of a complete vehicle.

Now in relatively simple experiments on a dynamical system involving one or perhaps two signal outputs, comparison with theory can be straightforward. For example, if the data is restricted to the history of a pitch angle oscillation, one might compare measured and predicted values of frequency and damping ratio. However, for the present project, which involves several signal outputs, a different approach has been adopted. This is to use the techniques of system parameter identification (SPI) to obtain from the data estimates of the coefficients of the differential equations that are believed to describe the vehicle dynamics. The evaluation of the accuracy of the theory is then made by comparing the theoretical values of these coefficients with those estimated from the data.

The problem may be illustrated by using an example. Consider the classic mass-spring-damper system described by the equation

$$m\ddot{x} + c\dot{x} + kx = f(t)$$

where $x(t)$ is the time varying displacement of the mass "m" that occurs in response to an input force $f(t)$. Assume that "m" is known, but the stiffness "k" and the damping "c" cannot be measured directly. Transducers are available to measure the quantities x, $\dot{x}$, $\ddot{x}$ and f at any instant of time $t_1 = t_2$, t_2 and so on. Hence, using a subscript "m" to denote a measured value, given data at time t_1 and t_2 one can write

$$m\ddot{x}_m(t_1) + c\dot{x}_m(t_1) + kx_m(t_1) = f_m(t_1)$$

$$m\ddot{x}_m(t_2) + c\dot{x}_m(t_2) + kx_m(t_2) = f_m(t_2)$$

This gives two linear algebraic equations for the two unknowns "c" and "k" so that the problem is solved. Even if transducers are available only to measure accelerations "x", displacements "x" and inputs "f", no difficulty arises in principle, because one can take additional measurements at time $t = t_1 + \delta t$ and $t = t_2 + \delta t$ to estimate velocities as follows:

$$\dot{x}_m(t_1) \cong \left\{ \frac{x_m(t_1+\delta t) - x_m(t_1)}{\delta t} \right\}$$

Now the task is greatly complicated by the fact that the transducer signals are invariably contaminated by noise, that the process of numerically differentiating the data can introduce large errors, and by other problems. However, SPI is a well established problem and a considerable body of theory is available. For example, the

literature on attempts to analyse data from flight tests of aircraft extends back some fifty years, and the techniques that are applied today are quite sophisticated.[7,8] Typically, both random process theory and matrix algebra are now used to minimize the impact of measurement errors and to allow treatment of complex systems. And, as in most fields of engineering analysis, the development of large scale digital computers has had a major impact on the choice of methods and on the size and complexity of the systems that can be investigated.

The primary purpose of this paper is to describe the development and application of an SPI procedure to the ACV dynamics experiments being conducted on the UTIAS track. Its consistency and validity is tested by comparing the SPI estimates of certain cushion properties such as pitch stiffness with those determined by separate and more direct experiments. A secondary purpose, brought into focus by these comparisons, is to assess the significance in ACV dynamics of the viscoelastic or stress relaxation properties of certain materials used to construct flexible skirts. This second point, and the related problem of dynamic scaling of model skirts is discussed below.

SKIRT SYSTEM USED IN PRESENT PROJECT

For our more recent experiments, the skirt installed on Vampire 1 is an uncompartmented segmented system, based on British Hovercraft Development Limited (HDL) ideas and developed by Hoverlift Systems of Calgary (HSL). Its overall geometry is much simpler than that of the multicell types tested previously at UTIAS. The geometry of the segments is depicted in Fig. 2.

A relatively straightforward theory for the pitch stiffness of this skirt has been developed. It is described in detail in Ref. 9 but, since it plays a basic role in the development of the present projects, it is described briefly here.

Figure 3 depicts the geometry of the skirt when the vehicle centre of mass is located at a height h_p above the ground and at a roll angle α or pitch angle θ.

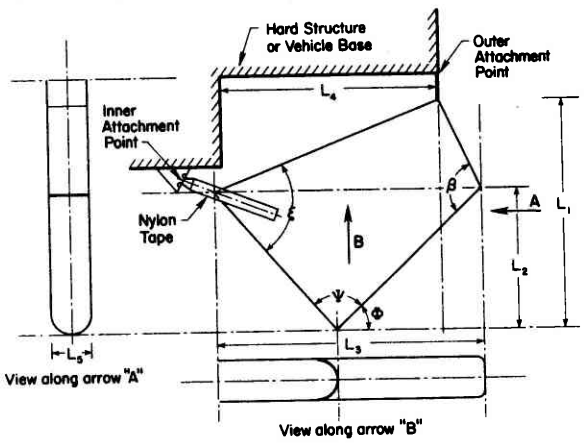


Fig. 2 Details of the HSL segments used at UTIAS.

The theory assumes that the skirt material is a weightless, completely inelastic membrane incapable of supporting any compression loads. This is the so-called "ideal model" material. It implies that the weight of the vehicle W is supported entirely by the cushion pressure p_c. Also it is assumed that the parts of the skirt that are forced into contact with the ground by the vehicle motion buckle only locally, so that the geometry of such quantities as the cushion footprint is defined by the intersection of the fully deployed skirt and the ground plane.

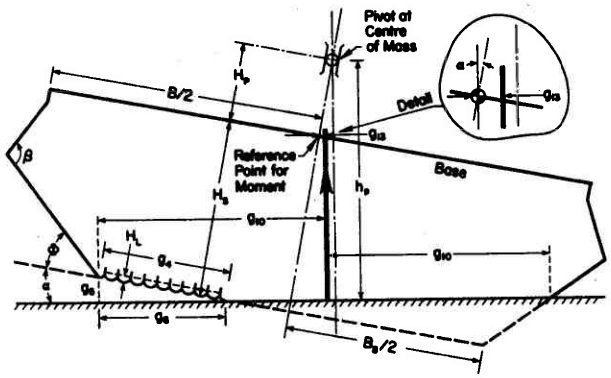


Fig. 3 Details of the geometry of the HSL skirt assumed for computing pitch and roll stiffness.

The theory is specified in terms of four coupled algebraic equations. The first of these equations is the known fan characteristic for delivery pressure p_f as a function of volume flow Q_f. Since, for the present system, the fan outlet pumps the air directly into the cushion, $p_f = p_c$. Also if the vehicle is hovering at some fixed θ and h_p, then $Q_f = Q_c$, the volume of air escaping from the cushion. Hence the measured characteristic can be fitted with a polynomial for p_c as a function of Q_c:

$$p_c = C_o + C_1 Q_c + C_2 Q_c^2 + C_3 Q_c^2 \qquad (1)$$

The second equation describes the cushion air escape process. Here it is assumed to be the usual Bernoulli law for orifice flows:

$$Q_c = C_D(\Phi) a_e(h_p,\theta)(2p_c/\rho)^{1/2} \qquad (2)$$

In this equation, C_D is the usual discharge coefficient, which is a function of the skirt taper angle Φ, $a_e(h_p,\theta)$ is the cushion air escape area, and ρ_a is the atmospheric density. The function $a_e(h_p,\theta)$ includes the two triangular areas, $g_5 g_6/2$ each in Fig. 3, a rectangular area $g_5 L_s$ at the front, plus an equivalent leak allowance H_L $(2g_4+L_s)$ associated with the rounded tips of the segment. The relationship of these quantities to the basic skirt geometrical parameters such as B_s and Φ is determined by trigonometry to obtain $a_e(h_p,\theta)$.

The third equation is the hover condition; if $a_f(h_p,\theta)$ is the cushion footprint area function

$$W = p_c a_f(h_p,\theta) \qquad (3)$$

The functional dependence of a_f on h_p and θ and the other skirt geometrical parameters is also determined by trigonometry.

Finally, the fourth equation is the moment equilibrium condition; if M is the known applied moment, this requires

$$M = Wg_{13}(h_p,\theta) = p_c a_f(h_p,\theta) g_{13}(h_p,\theta) \qquad (4)$$

where $g_{13}(h_p,\theta)$ is the location of the centroid of the cushion footprint relative to the centre of mass of the vehicle. As for $a_e(h_p,\theta)$ and $a_f(h_p,\theta)$, the dependence of g_{13} on h_p and θ and the skirt geometry is determined by trigonometry. Detailed development of the three functions $a_e(h_p,\theta)$, $a_f(h_p,\theta)$ and $g_{13}(h_p,\theta)$ is given in Ref. 9.

Solution of the four equations for the four unknowns (h_p, θ, p_c, Q_c) is obtained by digital computation. At the time of writing, numerical data for the Vampire 1 skirt had not been obtained. However, detailed experimental measurements have been obtained from a 2.44 × 1.22m test model; these are described in Ref. 9, and two examples are given in Figs. 4 and 5. The segments were made from an 0.01 mm thick nylon fabric coated with urethane, and the agreement between theory and experiment is very good, except at the larger pitch angles. The theory predicts that when the knee of the segment, defined by the angle β in Fig. 3, contacts the ground, the pitch stiffness decreases. In practice the segments buckle before this region is reached.

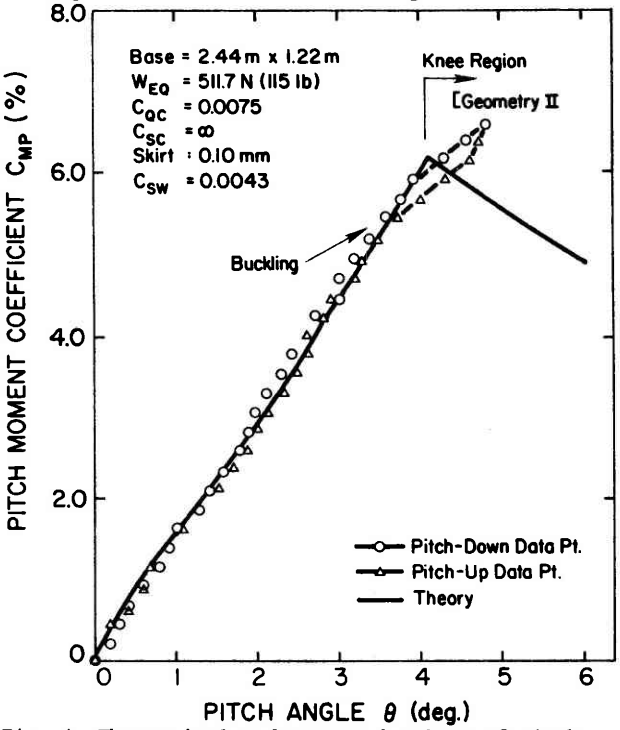


Fig. 4 Theoretical and measured values of pitch stiffness for HSL skirt. Skirt material is 0.10 mm urethane coated nylon with $\sigma = 0.076$ kg/m^2.

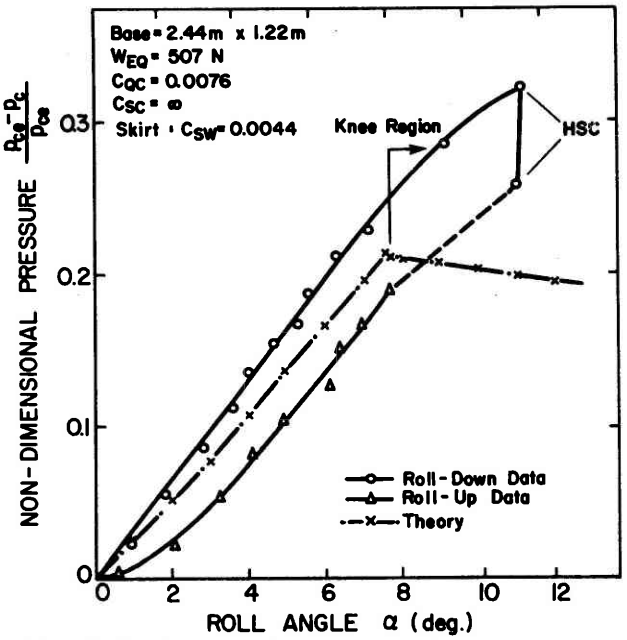


Fig. 5 Predicted and measured cushion pressure as a function of roll angle during roll-down to hard structure contact (HSC) and subsequent roll-up.

The quantity C_{QC} is the usual cushion flow coefficient, that is, $C_{QC} = Q_c(\rho_a/WA_{base})^{1/2}$, C_{SC} is the fan slope coefficient = $(Q_c/p_c)(dp_c/dQ_c)|_e$, and C_{SW} is the skirt material surface density coefficient = $\sigma A_{base}/W$. Here σ is the surface density of the skirt material (kg/m²); also note that $p_c = W/A_{base}$ approximately. The condition $C_{SC} = \infty$ denotes a constant volume flux air source. Figure 5, which gives an example of the experimentally measured and computed dependence of p_c as a function of roll angle α, shows that there can be a substantial pressure increase as the cushion rolls. A similar effect occurs in pitch.

It should be noted that an insight into the way this skirt works is sometimes obtained by assuming that it rolls or pitches about the tips of the segments on one side, or in Fig. 3, $g_5 = 0$. This gives the estimate $C_{MP} = (L_s\sin\theta)/(2L\tan\Phi)$ if the cushion footprint is assumed to be rectangular, and for the present skirt $dC_{MP}/d\theta = 0.90\%$ per degree. This is about 60% of that predicted by the present analysis. Also this simplified approach implies that the footprint area $a_f(h_p,\theta)$ increases as the model pitches, whereas both the present theory and the experiments imply that it decreases. Since almost all the model weight is being supported by the cushion pressure, and this quantity increases as the vehicle rolls or pitches, the hover condition implies that $a_f(h_p,\theta)$ must actually be decreasing as θ increases. Furthermore the simplified approach gives no information about the air escape area $a_e(h_p,\theta)$, a quantity needed for the development of the dynamics. Observation of both Vampire 1 and the 2.44 × 1.22m model shows that when the vehicle is pitching, the variation of $a_e(h_p,\theta)$ is large.

CHOICE OF SKIRT MATERIAL

Experimental measurements of the static pitch and roll stiffness characteristics of several UTIAS flexible skirt models have frequently displayed very significant hysteresis.[2,3] A recent example of the phenomenon, obtained from the 2.44 × 1.22m test model mentioned above, but with the 0.10 mm nylon-urethane segments replaced by segments made from 0.12 mm extruded polyethylene film, is given in Fig. 6. Note that the moment is higher for increasing θ than for decreasing θ, hence the hysteresis loop causes energy dissipation and thus is equivalent to damping. Various tests conducted at UTIAS have generally indicated that this phenomenon is usually, though not exclusively, associated with viscoelastic or other phenomena in the skirt material apparently triggered by skirt-ground contact.[2,3] Sliding friction between skirt and ground is not usually significant.[2,3,9]

Figure 7 gives the measured roll stiffness characteristic of Vampire 1 equipped with the HSL skirt. The material, which is an 0.46 mm thick neoprene coated nylon with σ = 0.380 kg/m², is the same as that used on NRC's HEX 4. This vehicle has

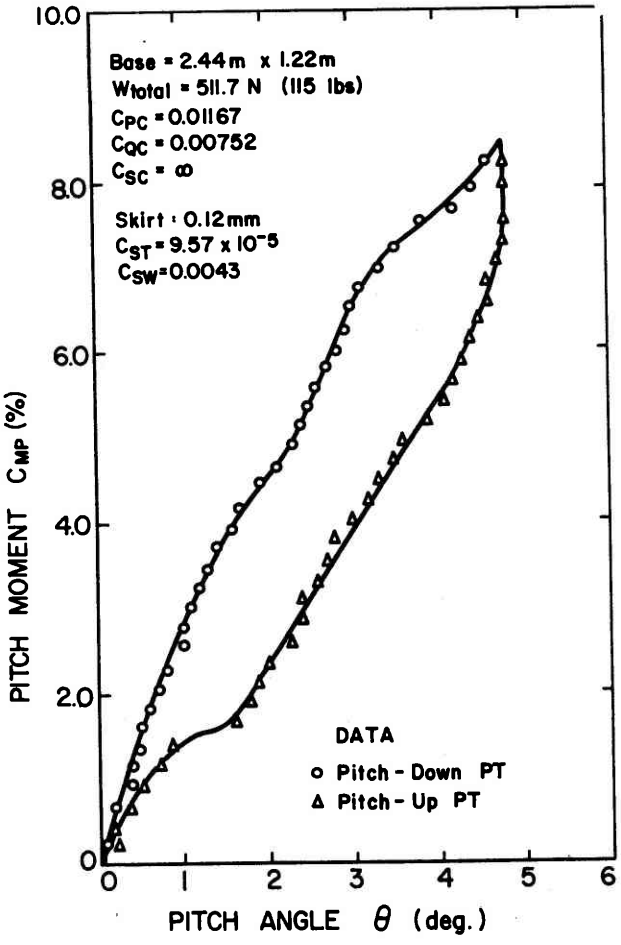


Fig. 6 Measured pitch stiffness for 2.44m × 1.22m model equipped with 0.12 mm thick extruded polyethylene film having σ = 0.118 kg/m².

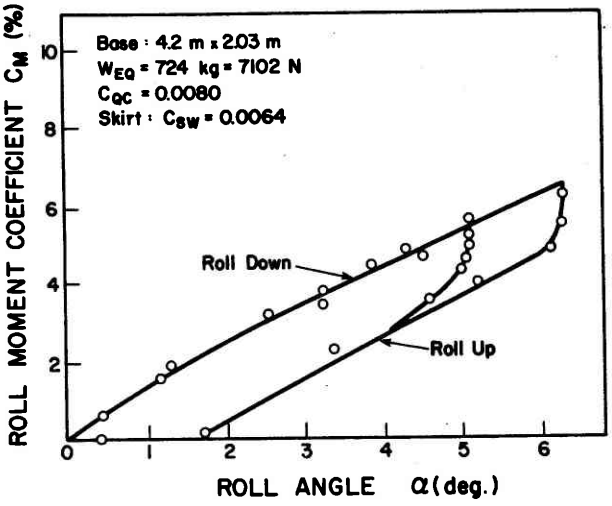


Fig. 7 Typical roll stiffness curve for the HSL skirt on Vampire 1, equipped with neoprene coated nylon 0.46 mm thick and with σ = 0.380 kg/m².

weight and planform dimensions very close to those of Vampire 1.[10]

We have to date not explored this phenomenon in depth, mainly owing to uncertainty about its practical significance, and to a lack of access on data for full scale vehicles. However, the relatively large size of Vampire 1 suggests that it could be significant. Moreover, a recent report on the stability and control of full scale vehicles in an operational context[11] describes static roll stiffness measurements for an amphibious vehicle having hysteresis comparable to that reported here.

A crucial question is the role that this hysteresis plays in the vehicle dynamics. Possible mechanisms include stress relaxation and plastic deformation in the material, or a combination of the two effects. The time constants associated with stress relaxation can be long,[6] so that the effect on the dynamics might then be less than would be implied from the static experimental results. If the hysteresis is caused mainly by plastic deformation during buckling in the parts of the skirt that are forced into contact with the ground, the effective dynamic damping could be larger than observed in the static tests. Hence it is not obvious what the magnitude of dynamic hysteresis effects will be, however, hysteresis of the magnitude displayed in Fig. 7 would, if it all interacted with the vehicle dynamics, have a major effect. Figure 8 shows the computed roll response of Vampire 1 to an initial roll angle α = 6.3° (HSC), obtained by assuming that the restoring moment history is that given by Fig. 7. For increasing α ($\dot{\alpha} > 0$) the "roll down" curve was used whereas for $\dot{\alpha} < 0$ the "roll up" curve was used. Clearly the hysteresis is contributing significantly to the damping. Large differences in the dynamic response of the 2.44m × 1.22m model to an initial disturbance in

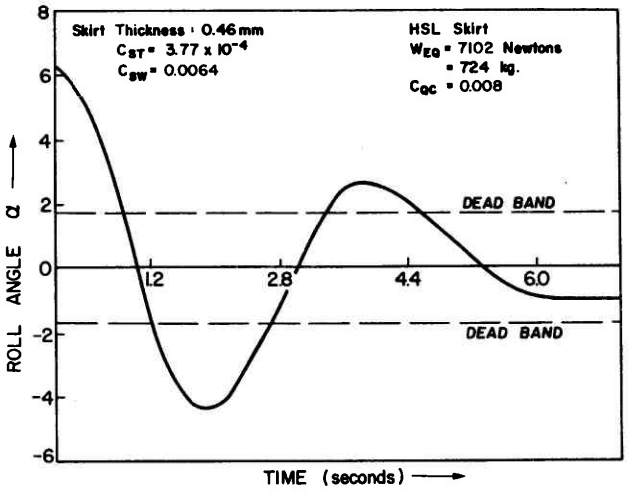


Fig. 8 Predicted roll response of Vampire 1 to the hysteretic damping shown in Fig. 7. For this calculation, no other damping was included.

pitch were observed for the two materials used to obtain the results given in Figs. 4 and 6, with the polyethylene segmented skirt exhibiting a much more heavily damped oscillation, as would be expected.[9] Hence the second purpose of the present project is the determination of the extent to which the hysteresis observed in static pitch stiffness measurements of Vampire 1 appears in the dynamics.

METHOD OF DATA ANALYSIS

Basic Concept

The procedure ultimately chosen for analysis of the test data is a response matching method. The concept is illustrated in Fig. 9. A time varying vector of inputs $\underset{\sim}{u}(t)$ to a dynamical system generates as an experimental response vector $\underset{\sim}{y}(t)$. This system response is assumed to be degraded by random measurement noise $\underset{\sim}{n}(t)$, which results in the measured response $\underset{\sim}{z}(t) = \underset{\sim}{y}(t) + \underset{\sim}{n}(t)$. This measured response is the data record to be analysed by the SPI procedure. Next, a form of a mathematical model for the system is assumed. That is, it is postulated that the dynamical system can be described by differential equations of a given order and degree, but that some or all of the coefficients are unknown. Then, for the control input used in the experiment, and with initial estimates of the vector of unknown coefficients $\underset{\sim}{c}$, the postulated mathematical model is used to calculate a response

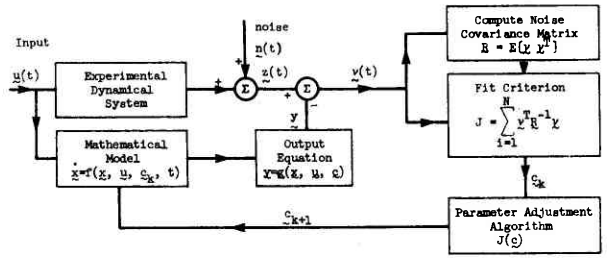


Fig. 9 Block diagram illustrating the concept of the SPI technique used in the present project.

$\underset{\sim}{y}_e(t)$. This calculated response is then compared with the measured response, to form an error or residual $\underset{\sim}{\nu}(t) = \underset{\sim}{z}(t) - \underset{\sim}{y}_e(t)$. A criterion function J is used to assess the "goodness of fit". This criterion is a function of the unknown parameters $\underset{\sim}{c}$. The values of the parameters $\underset{\sim}{c}$ are then adjusted — possibly by a random search, but usually by a more systematic technique — to improve the fit. Then, using the new values of $\underset{\sim}{c}$, namely $\underset{\sim}{c}_{k+1}$, response is calculated and compared with the measured response. The entire process is repeated a sufficient number of times to obtain an acceptable estimate of the unknown coefficients $\underset{\sim}{c}$.

Implementation

Development of the method divides naturally into three parts: (i) definition of the *form* of the response model, that is, selection of the model differential equations, and the determination of which parameters are to be treated as unknowns; (ii) selection of a *criterion function* by means of which the "goodness of fit" of the model response to the actual system response can be evaluated; (iii) selection of an *algorithm for adjustment of model parameters* to improve the fit of model to the data.

In connection with item (i), it is known that the final estimate of the unknown c obtained by this scheme is very sensitive to the form assumed.[8] Consequently, it does not replace the task of developing a mathematical model from a knowledge of the physics of the dynamical system. On the contrary, successful use of a SPI procedure relies heavily on the availability of a physical analysis to guide the choice of form. Also, it has been noted that if a complex model is used with only a limited amount of measurement information of low quality, an unreliable result will be obtained, if the method works at all.[12,13]

The selection of the form of the model, item (i) above, is discussed in the following section. The simplest possible criterion function, item (ii) above, is a least squares fit to the errors; that is, if data is available for a total of N time points t_i, and $\underset{\sim}{\nu}_i$ is the column vector of fit errors at time t_i, then a measure of the overall error at time t_i is the sum of the squares of the elements of $\underset{\sim}{\nu}_i$, $J_i = \underset{\sim}{\nu}_i^T \underset{\sim}{\nu}_i$. Hence a measure of the overall error is the sum of the J_i for each time point:

$$J(\underset{\sim}{c}) = \sum_{i=1}^{N} \underset{\sim}{\nu}_i^T \underset{\sim}{\nu}_i \qquad (5)$$

Here, the following ideas presented in the literature,[7,12] a maximum likelihood fit criterion was used. In its simplest form, this is

$$J(\underset{\sim}{c}) = \sum_{i=1}^{N} \underset{\sim}{\nu}_i^T \underset{\sim}{R}^{-1} \underset{\sim}{\nu}_i \qquad (6)$$

where $\underset{\sim}{R}$ is the covariance matrix of measurement noise $\underset{\sim}{n}(t)$, it is the square array given by

$$\underset{\sim}{R} = E\{\underset{\sim}{n}\,\underset{\sim}{n}^T\} = \sum_{i=1}^{N} \underset{\sim}{n}\,\underset{\sim}{n}^T \qquad (7)$$

This criterion may be derived by assuming that $\underset{\sim}{n}(t)$ obeys a multivariate Gaussian probability density law, and that the noise at each t_i is statistically independent of that at all other time points. If, in addition, the elements of $\underset{\sim}{n} = [n_\alpha]$ are statistically independent of each other, then $\underset{\sim}{R}$ reduces to the diagonal matrix whose elements are the standard deviations of the noise $\sigma_\alpha^2 = E\{n_\alpha^2\}$ and J_i becomes a weighted sum of squares:

$$J_i = \sum_\alpha \nu_\alpha^2/\sigma_\alpha^2\Big|_{t=t_i} \qquad (8)$$

Thus it may be seen that the maximum likelihood function improves the least squares estimate by weighting the response errors according to the quality of the data.

The parameter adjustment algorithm attempts to find the elements c_i of $\underset{\sim}{c}$ which minimizes the fit criterion or cost function J. Since the functional relationship $J(\underset{\sim}{c})$ is not explicitly known in this type of problem, it has to be determined numerically during the SPI analysis. One approach is to use what is known as a direct search technique.[13] An example of a direct search technique is as follows: given the k-th estimate $\underset{\sim}{c}_k$ of $\underset{\sim}{c}$, one proceeds by computing the values of J_k for a range of values of the first element c_{1k} of $\underset{\sim}{c}_k$. The value of $\underset{\sim}{c}_{1k}$ which gives a minimum value of J is then selected as the new value of $c_{1,k+1}$. The remaining elements of $\underset{\sim}{c}$ are then varied, one by one in sequence to obtain $\underset{\sim}{c}_{k+1}$. For the present problem, however, this is relatively inefficient.[13]

A technique frequently used for SPI searches is based on the well known Newton-Raphson algorithm for numerical solution of a set of coupled nonlinear algebraic equations.[13] Now a minimum of J occurs when $\nabla_c J$, the gradient of J with respect to $\underset{\sim}{c}$, is zero, that is, when

$$\nabla_c J = \underset{\sim}{g} \triangleq \left[\frac{\partial J}{\partial c_i}\right] = 0, \qquad i = 1, 2 \qquad (9)$$

The Newton-Raphson technique assumes that J can be approximated locally by a quadratic in $\underset{\sim}{c}$, in which case the new estimate of $\underset{\sim}{c}$ is given by

$$\underset{\sim}{c}_{k+1} = \underset{\sim}{c}_k - \underset{\sim}{G}_k^{-1}\,\underset{\sim}{g}, \qquad [\underset{\sim}{G}]_{ij} \triangleq \left[\frac{\partial^2 J}{\partial c_i \partial c_j}\right] \qquad (10)$$

As it stands this technique, which applies to any general function $J(\underset{\sim}{c})$ requires the inversion of a matrix of numerically computed second order derivatives and has other major difficulties, so that it is rarely used in this form. However, when J is essentially a sum of squares, as in Eq. (9), it can be modified to eliminate the need for second order differentiation, and to produce a particularly efficient algorithm known as the Gauss-Newton or Newton-Balakrishnan technique.[13] This was used in the present SPI analysis.

The SPI programme finally implemented was based on one compiled by Iliffe and Taylor.[14,15] The cost function J included a term to allow for the possibility that good estimates of some of the elements of $\underset{\sim}{c}$ are available. This is given in Appendix A, along with the adjustment algorithm. Also, the noise covariance matrix $\underset{\sim}{R}$ is not known initially, but has to be estimated and updated from the response error data as shown in Fig. 9, that is, $\underset{\sim}{R}$ is estimated by $E\{\underset{\sim}{\nu}\,\underset{\sim}{\nu}^T\}$ with $\underset{\sim}{R} = \underset{\sim}{I}$ for the first estimate.

Finally, it should be noted that the SPI programme compiled by Iliffe and Taylor[14,15] allows only the use of linear differential equations, $\dot{\underset{\sim}{x}} = \underset{\sim}{A}\,\underset{\sim}{x} + \underset{\sim}{B}\,\underset{\sim}{u}$, the response model. It uses the special properties of these equations to simplify the programme and make it more efficient. This poses a difficulty for the present project because hysteretic damping is inherently nonlinear; it implies that the hysteresis has to be modelled as an equivalent linear viscous damping. Although this is not very satisfactory, since it leads to prediction of unrealistic values of damping at oscillation frequencies substantially different from those encountered in the experiment, it was considered acceptable for the present exploratory investigation.

THEORETICAL MODEL OF PITCH-HEAVE DYNAMICS

Assumptions

The theoretical model of the dynamical response of Vampire 1 to a ramp disturbance has been developed by using the following assumptions:

(i) the vehicle moves at constant forward speed and is disturbed in pitch and heave only;
(ii) gyroscopic effects of the rotating parts of the vehicle such as fan and propeller are ignored;
(iii) the dynamic effects associated with the basic motion of the vehicle on a circular path around the track are negligible;
(iv) the assumptions used in the development of the static stiffness theory for this skirt apply and, in addition, the skirt material is so light that it can be assumed to be inertialess;
(v) the fan behaviour in the presence of variations of cushion pressure and cushion volume flow associated with the dynamics follows the measured static characteristic, that is, the fan behaves quasisteadily;
(vi) the usual assumptions for the basic cushion dynamics apply,[4] so that the cushion air compressibility can be modelled as a lumped pneumatic capacitance, and all air flow processes are incompressible and quasisteady;
(vii) additional skirt material hysteretic damping is modelled as an equivalent viscous damping.

Formulation

By assumption (v), the steady fan law, Eq. (1) applies at each instant in time

$$p_c(t) = C_o + C_1 Q_f(t) + C_2 Q_f^2(t) + \ldots \qquad (11)$$

except that $Q_f \neq Q_c$ in general, since the volume enclosed by the cushion V_c now varies with time. By assumptions (vi), cushion air escape law is the same as Eq. (2),

$$Q_c(t) = C_D a_e[h_p(t),\, \theta(t)]\sqrt{2p_c/\rho_a} \qquad (12)$$

but now the variables on which a_e depends, h_p and θ, are functions of time as determined by the

dynamics. The lift force generated by the cushion F is not now always equal to the vehicle weight, however, it is given by Eq. (3)

$$F(t) = p_c(t)a_f[h_p(t),\ \theta(t)] \tag{13}$$

Similarly the moment generated at each instant is given by the second form of Eq. (4)

$$M(t) = p_c(t)a_f(h_p,\ \theta)g_{13}(h_p,\ \theta) \tag{14}$$

The equations for the dynamics of the vehicle are now stated; these are Newton's law for the motion of the centre of mass of a rigid body applied to $h_p(t)$:

$$\frac{W}{g}\ddot{h}_p = F - W - \xi_h\dot{h}_p; \quad \dot{h}_p \equiv \frac{dh_p}{dt} \tag{15}$$

In this equation ξ_h is equivalent linear viscous damping modelling the hysteresis. The second equation is obtained from Euler's equations for rigid body rotation; it is, with I = pitch moment of inertia of the vehicle,

$$I\ddot{\theta} = M - \xi_\theta\dot{\theta} \tag{16}$$

The term $\xi_\theta\dot{\theta}$ models the hysteresis in pitch.

One more equation is required to couple the vehicle dynamics to that of the fluid flow processes. This is the cushion volume conservation law; if $V_c(h_p,\ \theta)$ is the volume enclosed by the skirt system and the vehicle hard structure, then

$$\frac{dV_c}{dt} + C_c\frac{dp_c}{dt} = Q_f - Q_c \tag{17}$$

in which C_c is the pneumatic capacitance given by

$$C_c = V_{ce}/\rho a^2 \tag{18}$$

The pneumatic capacitance of the cushion volume is included in the present investigation because of its well established fundamental role in the dynamical stability of cushion systems.[4] However some investigators have not included it,[16] and it appears that its omission may be reasonable provided that the vehicle operating conditions are not too near a stability boundary.

Dimensionless Form of Equations

The equations are now cast in dimensionless form as follows. If Q is some dimensional parameter or variable, then, according to the Π-theorem of dimensional analysis and choosing ρ_a, L and W as the reference variables having independent dimensions, the dimensionless equivalent, denoted by $\bar{(\ )}$, is given by

$$\bar{Q} = Q/\rho_a^{\alpha_1} L^{\alpha_2} W^{\alpha_3}) \tag{19}$$

where the exponents α_1, α_2 and α_3 are chosen to make the product $\rho_a^{\alpha_1} L^{\alpha_2} W^{\alpha_3}$ have the same dimensions as Q. The system differential equations become

$$\bar{p}_c = \bar{C}_o + \bar{C}_1\bar{Q}_f + \bar{C}_2\bar{Q}_f^2 + \ldots \tag{20}$$

$$\bar{Q}_c = C_D(2\bar{p}_c)^{1/2}\,\bar{a}_e(\bar{h},\ \theta) \tag{21}$$

$$\frac{d^2\bar{h}}{d\bar{t}^2} = \bar{g}[\bar{p}_c\bar{a}_f(\bar{h},\ \theta) - 1 - \bar{\xi}_h(d\bar{h}/d\bar{t})] \tag{22}$$

$$\bar{Q}_f - \bar{Q}_c = \frac{1}{\sqrt{2}}\left(\frac{d\bar{V}_c}{d\bar{t}} + \bar{C}_c\frac{d\bar{p}_c}{d\bar{t}}\right) \tag{23}$$

$$\bar{I}\frac{d^2\theta}{d\bar{t}^2} = \bar{p}_c\bar{a}_f(\bar{h},\ \theta)g_{13}(\bar{h},\ \theta) - \bar{\xi}_\theta\frac{d\theta}{d\bar{t}} \tag{24}$$

Note that the reference quantities ρ_a, L and W do not now explicitly appear in the equations, and the dimensionless equivalent of h_p is $\bar{h}$.

In the present investigation, ρ_a, L and W were chosen as reference variables because the pneumatic capacitance of the cushion was included in the model. An alternative and perhaps better choice might be to replace ρ_a by the acceleration due to gravity g.

Linearized Equations

Linear differential equations of the pitch-heave dynamics were obtained by considering small perturbations about the equilibrium point corresponding to h_p = constant = h_{pe}, $\dot{h}_p = 0$, $\theta = \dot{\theta} = 0$. Denote these equilibrium conditions by the subscript "e". The static equilibrium hover conditions imply

$$\bar{p}_{ce}\bar{a}_f(\bar{h}_e,\ 0) = 1, \quad \bar{M} = 0 \tag{25}$$

Let

$$\left.\begin{aligned} \bar{p}_c &= \bar{p}_c|_e(1 + \tilde{p}) \\ \bar{Q}_c = \bar{Q}_c|_e(1 + \tilde{q}_c), \quad \bar{Q}_f &= \bar{Q}_c|_e(1 + \tilde{q}_f) \\ \bar{h} &= \bar{h}|_e(1 + \tilde{h}), \quad \theta = \tilde{\theta} \end{aligned}\right\} \tag{26}$$

Introduce the definitions (26) into Eqs. (20) to (24), assume that $\tilde{p}$, $\tilde{q}_f$, $\tilde{q}_c$, $\tilde{h}$ and $\tilde{\theta}$ are small compared to unity, and omit products of these quantities to obtain the following linearized approximations. First, the fan law becomes

$$\tilde{p} = \bar{C}_{sc}\tilde{p}_f \tag{27}$$

where

$$\bar{C}_{sc} = \{(\bar{C}_1\bar{Q}_c + 2\bar{C}_2\bar{Q}_c^2)/\bar{p}_c)\}_e$$

and the notation $\{\ \}_e$ indicates that all quantities are evaluated at the equilibrium conditions. The cushion air escape law becomes

$$\tilde{q}_c = \frac{\tilde{p}}{2} + A_1\tilde{h} + A_2\tilde{\theta} \tag{28}$$

where the constants A_1 and A_2 are given by

$$A_1 = \left\{\frac{\bar{h}}{\bar{a}_e}\left(\frac{\partial\bar{a}_e}{\partial\bar{h}}\right)\right\}_e, \quad A_2 = \frac{1}{\bar{a}_e}\left\{\left(\frac{\partial\bar{a}_e}{\partial\theta}\right)\right\}_e \tag{29}$$

Newton's law for the vertical motion becomes

$$\ddot{\tilde{h}} = B_1\tilde{p} + B_2\tilde{h} + B_3\tilde{\theta} - B_4\dot{\tilde{h}} \tag{30}$$

where

$$B_1 = \{\bar{g}/\bar{h}\}_e, \qquad B_2 = \left\{\bar{g}\frac{\partial\bar{a}_f}{\partial\bar{h}}\right\}_e,$$

$$B_3 = \left\{ \frac{\bar{g}}{\bar{h}} \frac{\partial \bar{a}_f}{\partial \theta} \right\}_e, \qquad B_4 = \bar{\xi}_{\bar{h}} \bar{g}$$

Euler's equation for the pitching motion becomes

$$\ddot{\theta} = C_1 \tilde{h} + C_2 \tilde{\theta} - C_3 \dot{\theta} \tag{31}$$

where

$$C_1 = \left\{ \frac{\bar{h}}{\bar{I}} \frac{\partial \bar{g}_{13}}{\partial \bar{h}} \right\}_e, \qquad C_2 = \left\{ \frac{1}{\bar{I}} \frac{\partial \bar{g}_{13}}{\partial \theta} \right\}_e, \qquad C_3 = \frac{\bar{\xi}_\theta}{\bar{I}}$$

Finally, the cushion conservation law becomes

$$\tilde{q}_f - \tilde{q}_c = D_1 \dot{\tilde{h}} + D_2 \dot{\tilde{p}} \tag{32}$$

where

$$D_1 = \left\{ \frac{\bar{h}}{\bar{p}_c \bar{Q}_c} \right\}_e, \qquad D_2 = \left\{ \frac{\bar{C}_c \bar{p}_c}{\bar{Q}_c} \right\}_e$$

To cast this into matrix form $\dot{\underset{\sim}{x}} = \underset{\sim}{A}\, \underset{\sim}{x}$, substitute Eqs. (27) and (28) into (32) to obtain

$$\dot{\tilde{p}} = E_1 \tilde{p} - E_2 \tilde{h} - E_3 \tilde{\theta} - E_4 \dot{\tilde{h}} \tag{33}$$

where

$$E_1 = \left(\bar{C}_{sc}^{-1} - \frac{1}{2} \right) \left\{ \frac{\bar{Q}_c}{\bar{C}_c \bar{p}_c} \right\}_e, \qquad E_2 = \left\{ \frac{\bar{h}}{\bar{C}_p} \frac{\partial \bar{a}_e}{\partial \bar{h}} \right\}_e$$

$$E_3 = \frac{1}{\bar{C}_p} \left\{ \frac{\partial \bar{a}_e}{\partial \theta} \right\}_e, \qquad E_4 = \left\{ \frac{\bar{h}}{\bar{C}_c \bar{p}_c^{\,2}} \right\}_e,$$

$$\bar{C}_p = \frac{\bar{C}_c}{\bar{C}_D} \left(\frac{\bar{p}_{ce}}{2} \right)^{1/2}$$

Now, for simplicity, dropping the ($\tilde{}$) symbol, define

$$\underset{\sim}{x} = \begin{bmatrix} \dot{h} \\ \dot{\theta} \\ h \\ \theta \\ p_c \end{bmatrix}, \qquad \dot{\underset{\sim}{x}} = \begin{bmatrix} \ddot{h} \\ \ddot{\theta} \\ \dot{h} \\ \dot{\theta} \\ \dot{p}_c \end{bmatrix} \tag{34}$$

to give the required form

$$\dot{\underset{\sim}{x}} = \underset{\sim}{A}\, \underset{\sim}{x} \tag{35}$$

where the (5×5) system matrix $\underset{\sim}{A}$ has the following non-zero elements:

$$\underset{\sim}{A} = [a_{ij}] = \begin{bmatrix} a_{11} & 0 & a_{13} & a_{14} & a_{15} \\ 0 & a_{22} & a_{23} & a_{24} & 0 \\ 1 & 0 & 0 & 0 & 0 \\ 0 & 1 & 0 & 0 & 0 \\ a_{51} & 0 & a_{53} & a_{54} & a_{55} \end{bmatrix} \tag{36}$$

$$\left.\begin{aligned} a_{11} &= -B_4; \quad a_{13} = B_1; \quad a_{14} = B_3; \quad a_{15} = B_1 \\ a_{22} &= -C_3; \quad a_{23} = C_1; \quad a_{24} = C_2 \\ a_{51} &= -E_4; \quad a_{53} = -E_2; \quad a_{54} = -E_3; \quad a_{55} = E_1 \end{aligned}\right\} \tag{37}$$

These are the parameters which were to be estimated by the SPI procedure.

STATIC MEASUREMENTS

Pitch stiffness and other static cushion data was obtained by attaching a special harness system to the vehicle. This harness system, which is located in the Model Preparation Bay, constrains the vehicle to move only in pitch and heave. It uses linear and rotary ball bushings to eliminate sliding friction, and is designed to shat the axis of pitch rotation passes through the centre of mass of the vehicle.

In a particular experiment, QC was determined indirectly from the steady fan characteristic by measurement of fan speed and cushion pressure. The fan characteristic itself was obtained by removing the skirt and its base, sealing off the bottom of the plenum chamber and passing all cushion air through ducts attached at the rear of the vehicle to an ASME standard orifice plate installation. Fan speed was initially measured by using a stroboscope to count the blade passing frequency of the axial lift fan. More recently a photoelectric device has been installed in the fan annulus to detect blade passage; its output was read by a digital pulse counter-timer. Pitch angle and heave height were obtained by measuring the height above a datum of tabs attached to the four extremities of the vehicle. Prior to each experiment, accurately calibrated test weights were loaded on the vehicle at two special attachment points to obtain the desired operating gross weight W, and to trim the vehicle to zero pitch angle. Then to obtain pitch stiffness data, once the vehicle was on cushion and the required value of fan speed was attained, weights were transferred from one end to the other, one at a time.

A typical pitch stiffness curve obtained at a vehicle mass of 842 kg and fan speed N = 2000 rpm is given in Fig. 10. Stiffness curves for vehicle masses in the range 766 to 842 kg and fan speeds in the range $1800 \leq N \leq 2200$ were all very close to this curve. The slopes of these curves give $dC_{MP}/d\theta = (1.43 \pm 0.06)\%$ per degree, which may be compared with the predicted value for the 2.44m × 1.22m model of about 1.50% per degree.

All curves also displayed a well defined hysteresis equivalent to a pitching moment of $\Delta C_{MP} = 0.80 \pm 0.1\%$. Although previous work at UTIAS on this phenomenon showed that, for a given skirt material, ΔC_{MP} should decrease as vehicle weight increases, no clear-cut trend was observed in the present results, presumably owing to the relatively small range of vehicle weights used. Note also that, although the polyethylene material used to obtain the data presented in Fig. 6 had a value of C_{SW} which was only 67% of that for the Vampire 1 segments ΔC_{MP} is much larger. This is an example of the type of behaviour which leads us to conclude that the hysteresis is associated with properties of the skirt material and not sliding friction between the skirt and the ground.

Figure 11 shows the heave response that occurred

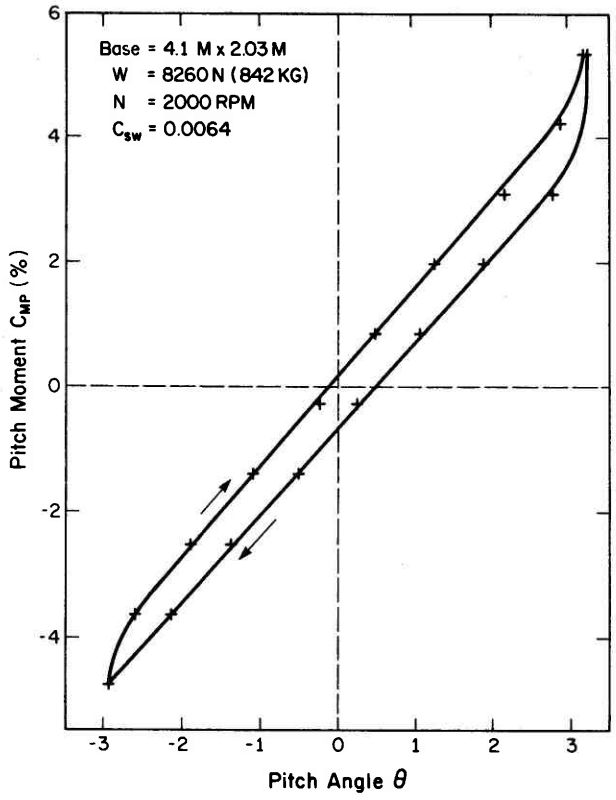


Fig. 10 A typical pitch stiffness curve for Vampire 1.

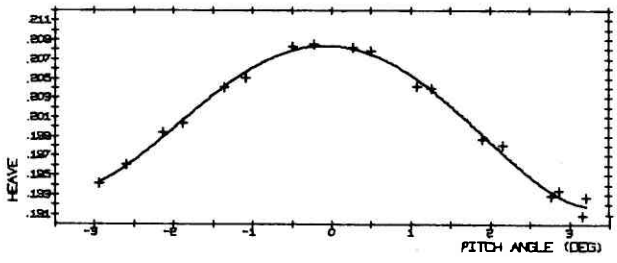


Fig. 11 Typical motion of centre of mass (h_p) at constant weight during a pitch test.

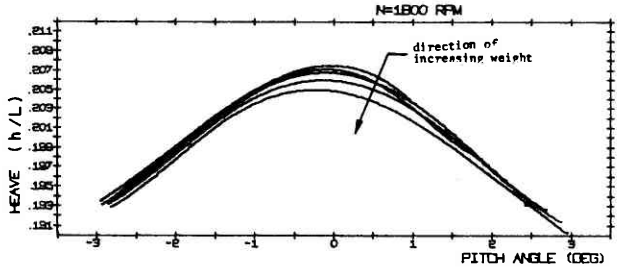


Fig. 12 Fitted curves for heave motion during pitch tests. The weights included are, in increasing order, 7518, 7700, 7887, 8074, 8261 Newtons.

during the pitch stiffness test undertaken to obtain the data shown in Fig. 10. It shows the large coupling between pitch and heave motion that occurs for this design of cushion. To obtain an estimate of heave stiffness at $\theta = 0$, the data in Fig. 11 and for other vehicle weights were each fitted with a polynomial by a least squares procedure. These fitted curves are shown in Fig. 12. The values of h_p/L at $\theta = 0$ according to these curves were used for computing heave stiffness.

DYNAMICS MEASUREMENTS

The basic experiment is straightforward. After the computer and DDAS have been powered up and given their initial instructions, both lift and propulsion engines are started. The computer is then instructed to sample data during a given time interval and to set signal gains at their desired values. After the vehicle has accelerated and lift-off is attained, the vehicle is flown around the track a sufficient number of times to stabilize the forward speed and to record all signal channel offsets. The ramps are then raised, and the computer is put in a holding mode. Data acquisition is then initiated by the operator just as the vehicle approaches the ramp.

Figure 13 shows a typical output voltage history for the rear TAS that was recorded during and immediately after flight over the ramp. For these initial experiments, no attempt was made to model and analyse the dynamical behaviour of the vehicle during the period in which it was traversing the ramp. Instead, a time point just after the rear TAS had left the ramp was selected to define initial conditions, and all previous data was discarded. That is, only time histories of the measured variables after this time point were used in the SPI analysis. One difficulty created by this approach is that some elements of the initial condition $\underset{\sim}{x}|_{t=0}$ become unknown parameters that have to be estimated by the SPI analysis.

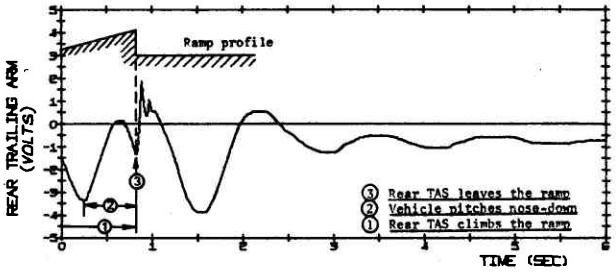


Fig. 13 Rear TAS response to ramp disturbance.

Figure 14 shows typical data obtained from one of the runs. The TAS voltages have been processed to obtain heave height h(t) and pitch $\theta(t)$ and roll $\alpha(t)$ but the other variables are direct readouts. Note that, although the ramps were set to initiate a disturbance in pure pitch, the vehicle always exhibited a large rolling motion. Also, of the measured variables, only h(t), $\ddot{h}(t)$, $\theta(t)$ and $\ddot{\theta}(t)$ were used in the SPI analysis. Before processing, all data was nondimensionalized according to the scheme discussed above.

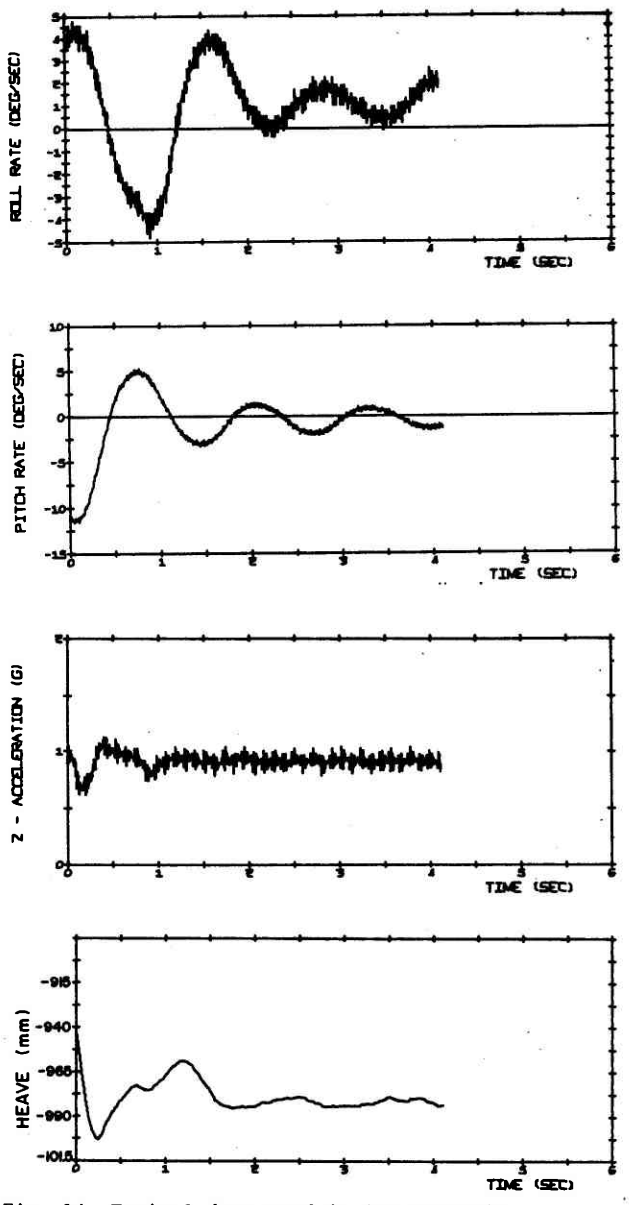


Fig. 14 Typical data used in SPI analysis.

In addition to the static measurements mentioned above, the pitch moment of inertia was determined in a separate experiment. For this experiment, the vehicle was supported well above ground level in the Model Preparation Bay by a shaft and roller bearing system, the axis of which passed through the centre of mass and which permitted the vehicle to rotate freely in pitch. An angular position transducer (RVDT) was attached to one of the shafts and accurately calibrated springs attached to the front and rear of the vehicle. A small amplitude lightly damped oscillation was then initiated, and the period of this oscillation was measured by an electronic digital counter-timer which monitored the output of the RVDT. It is noted that even at the amplitudes used in these tests, in which θ was always less than 1°, a dependence of the oscillation frequency on amplitude was detected. However the sensitivity of the instrumentation was such that the limiting frequency corresponding to very small oscillations could be estimated. The usual pendulum formulae were then applied to calculate I. The computed value of I corresponding to W = 6895 N was found to be 1243.7 kg-m². This is not much more than that obtained by assuming that it is a uniformly thick beam of length L, which is 975 kg/m².

The results of the SPI analysis are given in the fourth column of Table 1. They are discussed in conjunction with the values obtained from the static data in the next section. However an import test of the consistency of the procedure is to reconstruct the observed motion by using the SPI estimates of the unknown coefficients in a numerical simulation of the system dynamics. This has been done for the present experiment, and the results are given in Fig. 15, which compares measured (M) and reconstructed (S) data. The agreement is reasonably good.

Table 1

Table of Estimated and Calculated Parameters

Matrix Element	Parameter	Static Experiment	SPI	Notes
a_{11}	$-\bar{\xi}_h\bar{g}$	X	-0.636	Heave Damping
a_{13}	$\bar{g}\{\partial\bar{a}_f/\partial\bar{h}\}_e$	-1.10	-6.745	Heave Stiffness
a_{14}	$\tilde{g}\left\{\frac{1}{\bar{h}}\,\partial\bar{a}_f/\partial\theta\right\}_e$	0.033	0.742	
a_{15}	$\bar{g}/\bar{h}_e$	0.494	0.037	
a_{22}	$-\bar{\xi}_\theta/\bar{I}$	0.470	-0.423	Pitch Damping
a_{24}	$\frac{1}{\bar{I}}\{\partial\bar{g}_{13}/\partial\theta\}_e$	0.893	1.040	Pitch Stiffness
a_{51}	$\{\bar{h}/\bar{C}_c\bar{p}_c^{\,2}\}_e$	-139.4	-179.9	
a_{53}	$-\{\bar{h}(\partial\bar{a}_e/\partial\bar{h})/\bar{C}_p\}_e$	-174.6	-30.0	
a_{54}	$-\{\partial\bar{a}_e/\partial\theta\}_e/\bar{C}_p$	0.0	-3.2	
a_{55}	E_1	-4.58	-10.5	

COMPARISON OF DATA FROM STATIC AND DYNAMIC EXPERIMENTS

(i) Pitch Stiffness Coefficient, Element a_{24} of $\underset{\sim}{A}$ Matrix

The static pitch stiffness data for N = 2200 rpm give $\partial\bar{g}_{13}/\partial\theta \cong 0.83$, so that $a_{24} = 0.893$, compared to the SPI estimate of $a_{24} = 1.04$.

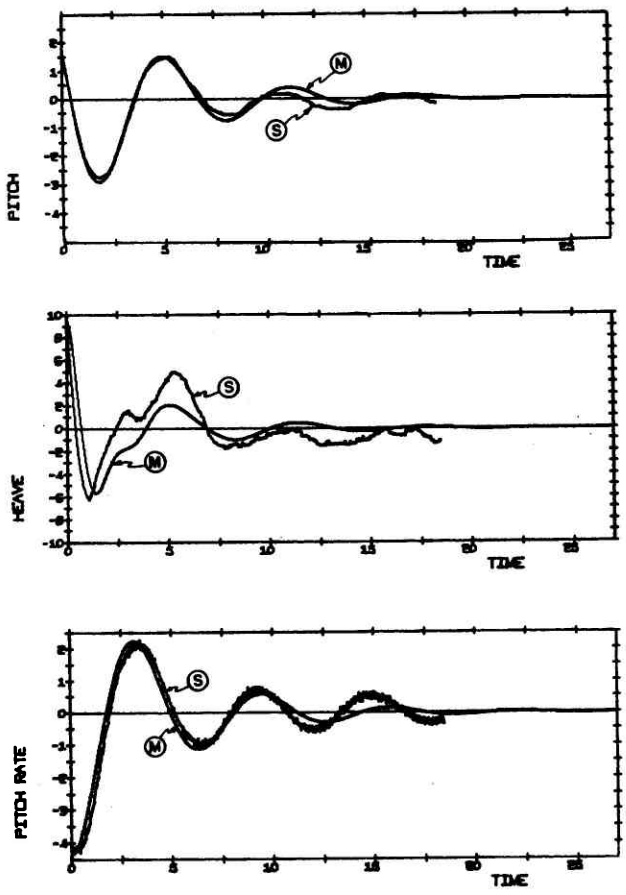


Fig. 15 Comparison of the experimental system response (S) and the response predicted by the mathematical model (M) using coefficients estimated by the SPI analysis.

(ii) Pitch Damping Coefficient, Element a_{22} of $\tilde{A}$ Matrix

Since, for a pitch oscillation, hysteretic damping of the type shown in Fig. 10 is proportional only to the amplitude of the oscillation, whereas for linear viscous damping it is proportional to both frequency and amplitude, an exact numerical comparison between the two for a decaying oscillation is not feasible. The most satisfactory approach is to compare the computed system response for the two types of damping. This was not done here, but the comparison of the measured and fitted response of pitch rate in Fig. 15 shows that the viscous damping realistically imitates the measured quantity. An approximate equivalence can be obtained by considering a steady state oscillation having representative values of amplitude and frequency, and by equating the work done by the two types of damping. Then with $\theta = \Theta \cos\omega t$, this leads to an estimate of $\bar{\xi}_\theta$ given by

$$\bar{\xi}_\theta = (2\Delta C_{MP})/(\pi\omega^2\Theta) \qquad (38)$$

For the first oscillation in Fig. 15, $\Theta \cong 1.2°$ and the nondimensional period T = 5.8. From the static experiments, at W = 7518N and N = 2200 rpm, $\Delta C_{MP} \cong 0.0075$. This gives an estimate of $\bar{\xi}_\theta/\bar{I} = 0.214$, which is a lower bound, since it is for the largest amplitude. If the average amplitude of θ is used, then the static data gives $\bar{\xi}_\theta/\bar{I} = 0.470$, which is closer to the SPI estimate of 0.423.

(iii) Heave Stiffness and Damping, Elements a_{11} and a_{13} of $\tilde{A}$ Matrix

From the definitions of nondimensional quantities

$$a_{13} = \bar{g}\left\{\frac{\partial \bar{a}_f}{\partial \bar{h}}\right\}_e = \frac{gL^2\rho_a}{W}\frac{\partial}{\partial \bar{h}}\left(\frac{W}{P_{ce}}\right)$$

Using this formula and data such as that given in Fig. 11, we obtained a static estimate of heave stiffness $a_{13} = -1.10$ as compared to the SPI estimate of -6.745. The discrepancy is thought to be caused by errors in the estimate of dh/dW obtained from the very small changes in L_p that occurred as a result of changes in W during the static experiments. Since no significant hysteresis could be detected in the static experiments, the static estimate of a_{11} is assumed to be zero. The SPI estimate is -0.636.

(iv) Footprint Function Derivative, Element a_{14} of $\tilde{A}$ Matrix

Since $a_f(h_p,\theta)$ is ideally an even function of θ, then $\partial a_f/\partial\theta = 0$ for $\theta = 0$. The nonzero value given by the SPI analysis may be due to a slight nose-up pitch attitude observed in the final data.

(v) Cushion Capacitance, Element a_{51} of $\tilde{A}$ Matrix

The nondimensional cushion capacitance $\bar{C}_c$ is given by

$$\bar{C}_c = \frac{WV_{ce}}{\gamma L^5(P_{ce} + P_a)}$$

where γ is the ratio of specific heats and P_a is the absolute atmospheric pressure. For Vampire 1, $\bar{C}_c = 1.86 \times 10^{-4}$ and $a_{51} = -139.4$ which may be compared with the SPI value of -180.

(vi) Air Escape Area Dependence on Pitch and Heave, Elements a_{53} and a_{54} of $\tilde{A}$ Matrix

Ideally, the air escape area $a_e(h_p,\theta)$ is an even function of θ, that is, $a_e(h_p,\theta) = a_e(h_p,-\theta)$ so $\partial a_e/\partial\theta\big| = 0$ at $\theta = 0$. Computations using the full nonlinear equations[9] for a_e show that it is a highly nonlinear function of θ, even for the small values of θ that occurred during the experiments. Furthermore, when $\theta = 0$ and $h_p = h_{pe}$, almost all of the segments are in partial contact with the ground, and the cushion air escapes through small triangular shaped regions formed by the adjoining segments and the ground. Hence $a_e(h_p,\theta)$ is also a highly nonlinear function of h_p in this region. Thus a linearization which, among other things, would approximate the θ-dependence of $a_e(h_p,\theta)$ by a constant is very unsatisfactory. Finally, $a_e(h_p,\theta)$ cannot be directly measured, but has to be inferred from a knowledge of Q_e and its dependence on p_{ce}, h_p and θ. We have yet to acquire sufficient data to adequately define this function. Thus although static data should give $a_{54} = 0$, the SPI estimate is -3.2, but no particular significance can be

attached to this discrepancy. All of the difficulties notwithstanding, an estimate of a_{53} was obtained from the static data.[9] This is at least of the same order as the SPI estimate.

DISCUSSION

Although we have obtained reasonably good agreement between the SPI estimates and statically measured values of the two quantities of major interest, namely pitch stiffness and pitch damping, the discrepancies in the other estimates indicate that much is yet to be done to make the work complete.

Improvements in the static experiments are required to obtain more accurate determination of heave stiffness and $a_e(h_p,\theta)$. This requires the accumulation of more experimental data. However, our current method of measuring air mass flow rates, by inference from a knowledge of cushion pressure and fan speed leads to large errors in some cases. The existing axial fan is stalled for a substantial part of the operating range of volume flows, and the flow in the inlet is partly recirculating, so that the inlet bell cannot be used to directly measure Q_e. The lift system is being redesigned to eliminate this and other problems.

Nonlinearities in the vehicle dynamics will have to be included in the SPI analysis. The attempt to interpret the hysteretic damping as an equivalent viscous damping is clearly an unsatisfactory artifice. The highly nonlinear behaviour of the air escape area function $a_e(h_p,\theta)$ should also be modelled realistically. However the task of developing SPI procedures for nonlinear systems incorporating such phenomena as hysteresis is not straightforward, it is a topic of current research in the field.[17]

Other improvements in the SPI procedure are also required. In general, it would only converge if very accurate initial estimates of the unknowns were used. In the literature[14,15] it is stated that this problem is most often caused by attempts to identify too many parameters. For example, improved convergence should be attained if the pitch stiffness is treated as a known parameter, determined either from the static experiments or the theory. Furthermore it is known that the nature of the control input to the experimental system can influence the chances of convergence,[12] and early work at UTIAS using simulated data showed that initial condition inputs similar to the type used in the present experiments gave convergence problems, whereas continuous control inputs did not.[18] Design of an appropriate input is one of our current major tasks.

It is noted above that during the experiments described here the vehicle executed a substantial rolling motion after passing over the ramps. Initially this was attributed to incorrect setting of yaw attitude, but we have subsequently concluded that gyroscopic torques generated by the lift fan is the major source of this extraneous motion.[9] The new lift system is a two stage contrarotating axial fan, and this choice of configuration was made initially to obtain reasonably high operating efficiencies at equilibrium values of Q_e much higher than can presently be attained. However, it features contrarotation and adjustable pitch blades to obtain high efficiency at the desired operating point.

CONCLUSIONS

The SPI technique for analysis of experiments on system and vehicle dynamics has been shown to be a useful, perhaps essential, tool in the interpretation of experiments on the dynamics of complete ACV's. However, it does not supplant the need for carefully defined experiments on particular aspects of the problem. On the contrary, it relies on these experiments and well defined theoretical analyses to provide satisfactory results and interpretations. Furthermore, it seems that air cushion technology provides new challenges to the technique, in that certain highly nonlinear features may have to be correctly represented rather than treated by the artifice of using "equivalent" linear systems.

Of more immediate interest to the ACV community are the conclusions we are now encouraged to make about the task of scaling skirt material for experimental testing of model ACV's. Although the UTIAS Circular Track project still requires a lot of work before it reaches a satisfying level of completion, it strongly reinforces inferences drawn from other UTIAS work: it is time to address the skirt material scaling problem in a thoroughly scientific way. What is happening in UTIAS experiments might conceivably be unrepresentative of full scale behaviour If these effects are important at full scale, then great care has to be exercised in the choice of model material. If they are not, which we now think unlikely, great care is still required to adequately choose model material.

NOMENCLATURE

Roman

a	atmospheric sound speed
$\underset{\sim}{A}$	system matrix for linear model of dynamics
A_{base}	area of base of vehicle = BL = 2.06×4.08m
$a_e(h_p,\theta)$	cushion air escape area function
$a_f(h_p,\theta)$	area of cushion footprint
B	width of vehicle base
B_s	width of cushion footprint at $\alpha = \theta = 0$
$\underset{\sim}{c}$	column vector of unknowns in SPI analysis
$\tilde{C}_o$, C_1, C_2	coefficients in empirically fitted curves of steady state fan characteristic $p_f = f(Q_f)$
C_c	pneumatic capacitance of cushion volume $= V_{ce}/\rho a^2$
C_D	volume flow discharge coefficient in Bernoulli model of efflux
C_{MP}	pitch moment coefficient, $C_{MP} = M/WL$
C_{SC}	fan law slope coefficient, $C_{SC} = (Q_f/p_f)\cdot(dp_f/dQ_f)$
C_{SW}	skirt material weight coefficient, $C_{SW} = \sigma A_{base}/W$
F	vertical force generated by cushion pressure
$g_i(h_p,\theta)$	sequence of functions describing cushion geometry when rolled or pitched. See

Fig. 3. g_{13} is location of centroid of cushion footprint

h_p height of centre of gravity above datum
I pitch moment of inertia of vehicle
$J(\underset{\sim}{c})$ cost function in SPI procedure
L length of vehicle
M moment about centre of mass generated by cushion pressure
$\underset{\sim}{n}(t)$ system measurement noise
$\underset{\sim}{p}_c$ cushion pressure = fan delivery pressure p_f for this skirt
Q_c volume flow from cushion to atmosphere
Q_f volume flow delivered by fan
$\underset{\sim}{R}$ noise covariance matrix, $\underset{\sim}{R} = E\{\underset{\sim}{n}\ \underset{\sim}{n}^T\}$
t time
$\underset{\sim}{u}(t)$ control input vector in linear model $\dot{\underset{\sim}{x}} = \underset{\sim}{A}\ \underset{\sim}{x} + \underset{\sim}{B}\ \underset{\sim}{u}$
V_c cushion volume
$\underset{\sim}{v}(t)$ experimental response vector
W gross weight of cushion
$\underset{\sim}{x}(t)$ output of dynamical system
$\underset{\sim}{y}(t)$ computed response in SPI procedure
$\underset{\sim}{z}(t)$ measured response including noise

Greek

α roll angle
ΔC_{MP} moment coefficient measurement of hysteresis magnitude
θ pitch angle
Θ amplitude of pitch oscillations
$\underset{\sim}{\nu}(t)$ response error in SPI procedure
ξ_h, ξ_θ additional equivalent linear damping terms to model skirt hysteresis
ρ_a atmospheric density
Φ segment angle relative to ground
ω circular frequency

Superscripts and Subscripts

e equilibrium at $\theta = 0$ and $h_p = h_{pe}$
i individual terms in cost function sum $J = \sum_{i=1}^{N} J_i$
k k-th iteration of $\underset{\sim}{c}$ vector
$(\bar{\ })$ nondimensional quantity
$(\tilde{\ })$ linearized perturbation

ACKNOWLEDGEMENTS

This project was made possible by the substantial and sustained support of two Canadian Government agencies. The National Research Council of Canada (NRC) provided the funds for construction of the Circular Track, and NRC and its successor in university research funding, the Natural Sciences and Engineering Research Council, have provided both Operating Grants (A3378) and Core Grants (A1613) over the years. Transport Canada's Transportation Development Centre (TDC) has supported the work continuously from its inception through contracts that have allowed us the flexibility to evolve the project in a way that is appropriate to a university environment, and which will enhance the chances of long term benefit to the ACV community. The support and encouragement of Mr. P. L. Eggleton and Mr. J. E. Laframboise of TDC, and Mr. H. S. Fowler of NRC is also gratefully acknowledged. The first author would also like to take this opportunity to express his gratitude to Dr. G. N. Patterson, Founding Director of UTIAS, for the opportunity to work at the Institute, and to senior members of the UTIAS staff who provided well conceived advice and encouragement through some very difficult times.

REFERENCES

1. Ribner, D. B., "A Remote Data Acquisition and Control System", Department of Electrical Engineering, University of Toronto, M.A.Sc. Thesis, July 1980.

2. Sullivan, P. A., Hinchey, M. J., and Delaney, R. G., "Static Roll Stiffness Characteristics of Two Multicell Air Cushion Systems", Journal of Terramechanics, Vol. 15, No. 1, 1978, pp. 15-41.

3. Sullivan, P. A., Hinchey, M. J., Parravano, J. G., and Murra, I., "Research on the Stability of Air Cushion Systems", Institute for Aerospace Studies, University of Toronto, Report No. 238, Nov. 1979.

4. Sullivan, P. A., Hinchey, M. J., and Green, G. M., "A Review and Assessment of Methods for the Prediction of the Dynamic Stability of Air Cushions", Journal of Sound and Vibration, to be published.

5. Hinchey, M. J., "Heave Instabilities of Amphibious Air Cushion Suspension Systems", Institute for Aerospace Studies, University of Toronto, Report No. 246, Nov. 1980.

6. Graham, T. A., "The Effects of Skirt Material Choice on the Heave Stability of an Air Cushion", Institute for Aerospace Studies, University of Toronto, M.A.Sc. Thesis, Oct. 1980.

7. Bekey, G. A., "System Identification — An Introduction and a Survey", Simulation, Vol. 15, No. 4, Oct. 1970, pp. 151-156.

8. Gelb, A., et al., Applied Optimal Estimation, M.I.T. Press, Massachusetts Institute of Technology, Cambridge, 1974.

9. Sullivan, P. A., et al, "Research on Air Cushion Stability — 1979 Report, Transportation Development Centre, Transport Canada, Montreal, Report TP3109E, Jan. 1982.

10. H. S. Fowler, National Research Council of Canada, Private Communication.

11. ———, "Stability and Control of Hovercraft: Notes for Commanders", United Kingdom Department of Industry Ship and Marine Technology Requirements Board BHC SP4432, 1980.

12. Stephner, D. E., and Mehra, R. K., "Maximum Likelihood Identification and Optimal Input Design for Identifying Aircraft Stability and Control Derivatives", National Aeronautics and Space Administration, Contractor Report CR2200, 1973.

13. Dixon, L. C. W., Nonlinear Optimization, Crane, Russak and Company, New York, 1972.

14. Taylor, L. W., and Iliffe, K. W.,"System Identification Using a Modified Newton-Raphson Technique — A Fortran Programme", National Aeronautics and Space Administration, Technical Note TND 6734, 1972.

15. Iliffe, K. W., and Taylor, L. W., "Determination of Stability Derivatives from Flight Data Using a Newton-Raphson Minimization Technique", National Aeronautics and Space Administration, Technical Note TND 6579, 1973.

16. Doctors, L. J., "Nonlinear Motion of an Air Cushion Vehicle Over Waves", Journal of Hydronautics, Vol. 9, No. 2, 1975, pp. 49-57.

17. Andronikou, A. M., Bekey, G. A., Masri, S. F., "Identification of Nonlinear Hysteretic Systems Using Random Search", Proceedings of the Sixth International Federation on Automatic Control Symposium on Identification and System Parameter Identification, Vol. 1, pp. 263-268, June 1981.

18. Hartmann, P. V., "Application of System Parameter Identification Methods to the Determination of Dynamic Pitch-Heave Characteristics of an Air Cushion Vehicle", Institute for Aerospace Studies, University of Toronto, M.A.Sc. Thesis, Oct. 1979.

AN OVER-VIEW OF UTIAS RESEARCH ON THE DYNAMIC STABILITY OF AIR CUSHION VEHICLES

M. J. Hinchey

Institute for Aerospace Studies
University of Toronto
Toronto, Canada

ABSTRACT

Dynamic instabilities have been encountered by a number of Canadian operators of air cushion vehicles. This paper presents an over-view of research at the University of Toronto, Institute for Aerospace Studies (UTIAS), dedicated to understanding the phenomenon. It includes a brief review of theoretical and experimental work on the destabilizing effect of cushion air supply ducts. The duct-plenum system is shown to behave as an Helmholtz resonator with the slug of air in the duct oscillating on the plenum air spring. For this work, a unique facility was developed which used a large hollow sphere as a pneumatic filter to isolate the duct-plenum system from the fan. The paper also outlines recently completed work on limit cycle oscillations, skirt material damping, large air cushion platforms, and air cushions hovering over water.

1. INTRODUCTION

Research at UTIAS on the dynamic stability of air cushions, motivated by the field experience of a number of Canadian operators, has been going on since 1975. The dynamic instabilities encountered are self-excited and are most often just a translation in the vertical direction, that is, a pure heave, but other more complex motions have also been observed. They can cause operational difficulties and in extreme cases lead to destruction of the vehicle. Furthermore, the limited amount of evidence available from field operations indicates that their onset may be governed by many factors. The present paper gives an over-view of the UTIAS research effort. The major research objective has been and still is to identify the various factors affecting stability. A second and broader aim is to devise a series of experiments which critically test the usefulness of available mathematical models of air cushion dynamics. This is motivated by the lack of such data in the available literature.

Our initial theoretical work used the lumped capacitance model.[1,2] This model yields important insights and is described briefly below in Section 2. It assumes the cushion air to be compressible and because of this it is the simplest model capable of predicting stability. However, it does have a number of limitations. Section 3 below is a review of the author's Ph.D. research in which a major effort was directed towards coming to terms with these limitations. Section 4 describes some recently completed work while Section 5 outlines work in progress.

2. THE LUMPED PNEUMATIC CAPACITANCE MODEL

Tulin[1] was the first to analyze the dynamic stability of an air cushion vehicle. He considered a peripheral jet machine and found that it could self-oscillate in heave and this was due primarily to a force-motion phase lag associated with cushion air compressibility. Ribich and Richardson[2] considered plenum as well as peripheral jet machines. They also pointed out the importance of the phase lag associated with compressibility and thus the necessity of keeping the enclosed volume as small as possible. They noted that management of the elastic properties of the skirt might be used to counteract compressibility and thus improve stability.

The stability calculations made by Tulin[1] and Ribich and Richardson[2] were based on a lumped pneumatic capacitance model. Because of the important insights it yields, this model is outlined below for a simple single cell air cushion, free to move in heave only.

The air in the cushion volume is assumed to be compressible and at any instant in time the pressure is assumed to be uniform throughout the volume. Thus, one can write the conservation equation

$$\frac{d}{dt}(\rho V_c) = \dot{M}_{in} - \dot{M}_{out} \tag{1}$$

where ρ is the air density, V_c is the volume, and $\dot{M}_{in}$ and $\dot{M}_{out}$ are the air mass flow rates into and out of the volume respectively. The effects of internal flows such as jets and vortices are assumed negligible. It is further assumed that the air pressure and density changes are related by polytropic equation of state

$$\frac{P}{\rho^n} = \text{constant} \tag{2}$$

where n is assumed to be equal to γ, the ratio of specific heats (isentropic). This and the ideal gas law $P = \rho RT$ allows one to write

$$\dot{P} = \gamma RT\dot{\rho} \tag{3}$$

For amphibious vehicles, the pressure and temperature perturbations are usually small relative to atmospheric conditions. Thus

$$\dot{P} = \dot{p} = a^2\dot{\rho} \tag{4}$$

where $a = \sqrt{\gamma RT}$ is the speed of sound in air. With this, the conservation equation reduces to

$$\frac{V_c}{\rho a^2}\frac{dp_c}{dt} = (Q_{in} - Q_{out}) - \frac{dV_c}{dt} \tag{5}$$

where Q_{in} and Q_{out} are volume flow rates. These flows are assumed to be governed by steady inviscid orifice flow laws applied quasi-statically in time. For amphibious vehicles, gauge pressures are usually low enough that the flows can be assumed incompressible, in which case

$$Q_{in} = C_{df}A_f\sqrt{\frac{2(p_f - p_c)}{\rho}}$$
$$Q_{out} = C_{da}\ell h\sqrt{\frac{2p_c}{\rho}} \tag{6}$$

where p_c is the gauge cushion pressure, p_f is the gauge fan pressure, A_f is the inlet orifice area, ℓ is the perimeter of the cushion at ground level, h is the hover-gap (assumed uniform) and C_d is an orifice flow discharge coefficient. The quasi-static law is based on Euler's equation for flow along an orifice streamline

$$\rho\frac{\partial V_s}{\partial t} + \rho V_s\frac{\partial V_s}{\partial s} + \frac{\partial p}{\partial s} = 0 \tag{7}$$

It is assumed that the flow is steady and ρ is constant. With this, Euler's equation reduces to

$$\rho V_s\frac{dV_s}{ds} + \frac{dp}{ds} = 0 \Rightarrow \frac{1}{2}\rho V_s^2 + p = C \tag{8}$$

which is Bernoulli's equation.

Another assumption is that the pressure-flow operating point of the fan moves along its static characteristic quasi-statically in time, where, in general, the static characteristic is a nonlinear relationship of the form

$$p_f = C_o + C_1Q_f + C_2Q_f^2 + \ldots + C_nQ_f^n \tag{9}$$

where $Q_f = Q_{in}$. Unsteady blade aerodynamics and oscillatory volute flow are ignored.

The cushion volume V_c is assumed to be made up of

$$V_c = V_o + Sh + f(p_c) \tag{10}$$

where S is the pressurized support area, V_o is a fixed volume component, Sh is an active component produced by the vehicle heave motion, and $f(p_c)$ is a flexibility component for which it is assumed that the skirt responds quasi-statically in time to temporal variations in cushion pressure. Inertial and hysteretic behaviour are ignored. To simplify the present discussion, flexibility effects on skirt height and support area are also ignored. It will be shown later that its effect on skirt height can be considerable.

Finally, Newton's second law gives for the heave displacement

$$m\frac{d^2h}{dt^2} = Sp_c - mg \tag{11}$$

where m is the suspension mass and g is the acceleration due to gravity.

Using matrix notation, the lumped parameter equations can be rewritten in the compact form

$$\dot{\underline{X}} = \underline{f}(\underline{X}) \qquad t \geq t_o \tag{12}$$

for which the most useful definition of stability is that due to Liapunov.[3,4] By this, an equilibrium state of the system is considered locally asymptotically stable if the system gradually returns to this state after being perturbed slightly from it. The equilibrium is said to be critically stable if the response neither grows nor decays. Local stability can be studied by using the linear approximation

$$\dot{\underline{X}} = \underline{A}(\underline{X} - \underline{X}_e) \tag{13}$$

where

$$\underline{f}(\underline{X}) = \underline{A}(\underline{X} - \underline{X}_e) + \underline{n}(\underline{X} - \underline{X}_e) \tag{14}$$

provided that in the vicinity of the equilibrium state the nonlinear terms $\underline{n}(\Delta\underline{X})$ are small relative to the linear terms. For a particular state to be locally asymptotically stable, the real part of each eigenvalue of the $\underline{A}$ matrix must be negative. This can be checked, without actually solving for the eigenvalues, λ, by using the Routh-Hurwitz criteria, which work with the coefficients in the characteristic equation obtained by expanding the $|\underline{A}-\lambda\underline{I}|$ determinant.

The Routh-Hurwitz criteria yield stability boundary equations of the form

$$p_{ce} = ftn(h_e) \tag{15}$$

where p_{ce}, the equilibrium cushion pressure, is directly proportional to the gross weight supported by the cushion, while h_e, the equilibrium gap, is a measure for a given operating terrain of the lift air needs. For a constant pressure fan characteristic, one obtains for a rigid skirt case the stability requirement[5]

$$p_{ce} \leq \frac{\rho a^2}{2}\left(1 + \frac{C_{df}^2A_f^2}{C_{da}^2\ell^2h_e^2}\right)\frac{h_e}{h_s} \tag{16}$$

where h_s is the skirt height, while for a constant flow source, one obtains[5]

$$p_{ce} \leq \frac{\rho a^2}{2}\frac{h_e}{h_s} \tag{17}$$

Note how geometrically similar cushions operating

at a geometrically similar gap would be unstable above the same cushion pressure. This presents a problem for scaling up to large sizes because it means that the stability pressure would not scale up but would be limited to that of geometrically scaled models. The two relationships given above are shown schematically in Figure 1, where the hatched side of each curve indicates an unstable region. The figure shows that a constant pressure source gives a much larger stable pressure-flow region than a constant flow source. It suggests that some sort of control (e.g., fan speed, inlet area, blade pitch angle) which could make the fan behave dynamically as a constant pressure source would be desirable. Note that if the cushion air was incompressible ($a = \infty$), the critical stability pressure for the rigid skirt case would be infinite.

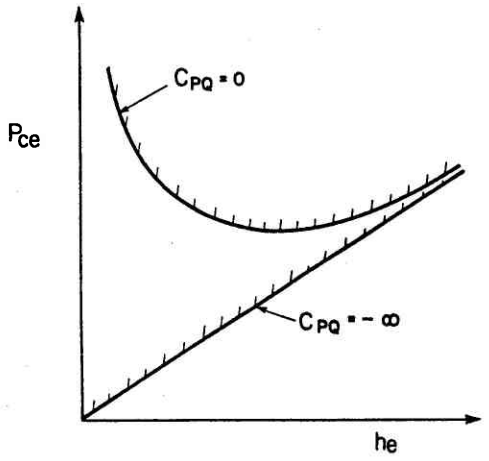


Fig. 1 Heave stability boundaries for a single cell air cushion

For the flexible skirt case, the stability pressure could be made infinite by making the effective capacitance equal to zero

$$C_{eff} = C_c + C_f = 0 \qquad (18)$$

where

$$C_c = \frac{V_{ce}}{\rho a^2}, \qquad C_f = \frac{dV_c}{dp_c}\Big|_e \qquad (19)$$

In other words, skirt flexibility would have to be manipulated, either passively or actively, to counteract the destabilizing lag effect of cushion air compressibility.[5]

3. UTIAS: EARLY WORK

As mentioned in the Introduction, an important objective has been and still is to devise a series of experiments which critically test the available mathematical models and their inherent assumptions. Some success towards meeting this objective is described below.

3.1 Duct Effects

A major effort was directed towards understanding the effects of unsteady duct flow on heave stability.[5-7] Various acoustic duct models were considered. However, it was found that for amphibious vehicles the duct effect was mainly a lumped inertance effect. The lumped inertance model is based on Newton's second law applied to the mass of air in the duct. In linearized form, the governing equation for the single cell duct-plenum system shown in Figure 2 is

$$\frac{d\Delta Q_d}{dt} = \frac{A_d}{L_d \rho}(\Delta p_{df} - \Delta p_{dc}) = \frac{\Delta p_{df} - \Delta p_{dc}}{I_d} \qquad (20)$$

where ΔQ_d is the duct flow perturbation, A_d is the duct cross-sectional area, L_d is the duct length, ρ is the air density, I_d is the lumped inertance, and Δp_{df} and Δp_{dc} are the pressure perturbations at the fan end and the cushion end of the duct respectively. Typical results obtained using a lumped capacitance cushion model and an acoustic duct model are shown in Figure 3, where again the hatched side of each curve indicates an unstable region. To generate the results in Figure 3, a $1.415 m^3$ duct volume was stretched into a series of ducts having different length-to-diameter ratios. The basic system dimensions are given in Table 1. All acoustic and lumped inertance results were obtained using a constant pressure source which for stability represents an ideal. The two curves for case 3 are just parts of a single boundary such as that for case 4; similarly for case 2. Note the agreement between the acoustic and lumped inertance results obtained for case 3. Note also how at low hovergaps the ducting introduces an unstable region which becomes larger as the duct length-to-diameter ratio is increased. It was found that at the low hovergaps the duct-plenum

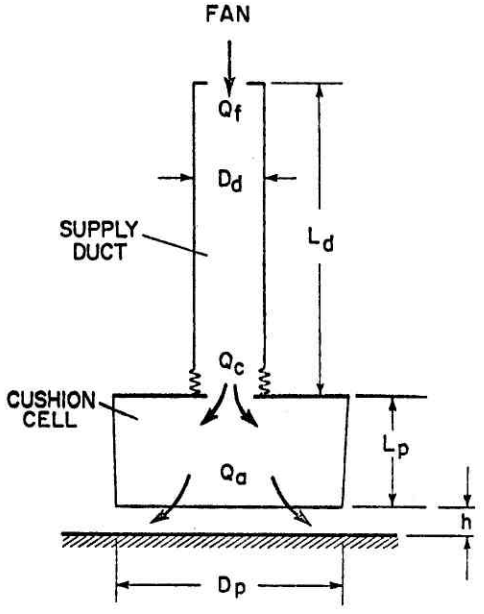


Fig. 2 Duct-plenum model

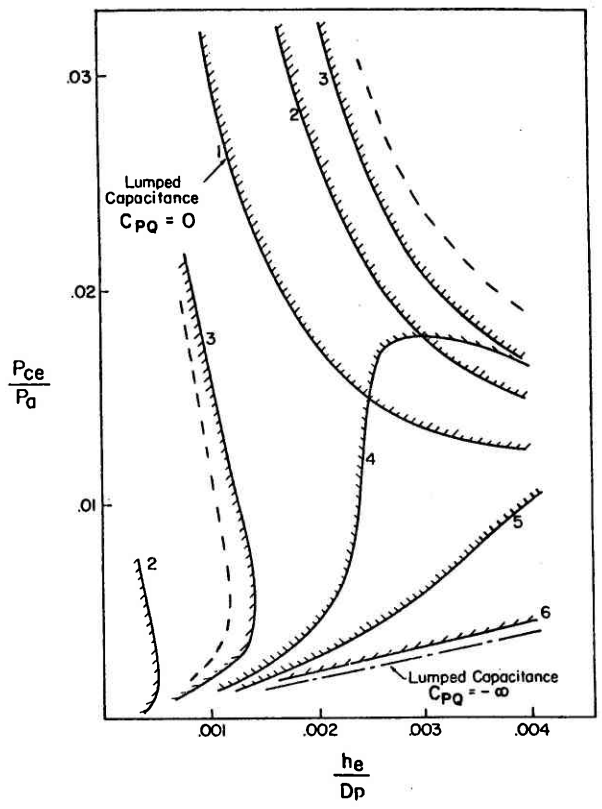


Fig. 3 Heave stability boundaries showing duct effect
Full line: acoustic
Dashed line: lumped inertance for case 3

Case	1	2	3	4	5	6
L_d/D_d	1/8	4	8	12	16	64

Diameter of cell	=	1.83m (6 ft)
Height of cell	=	0.915m (3 ft)
Duct volume	=	1.415m^3 (50 ft^3)
Fan orifice diameter	=	0.304m (1 ft)
Cushion orifice diameter	=	0.304m (1 ft)
Duct length-to-diameter ratio	=	Variable
Duct friction factor	=	0.0
Polytropic exponent	=	1.4

Table 1 Dimensions of duct-plenum model

system tended to act as an Helmholtz resonator; the slug of air in the duct tended to oscillate on the plenum air spring. The oscillation frequency was approximately that of the classical Helmholtz resonator

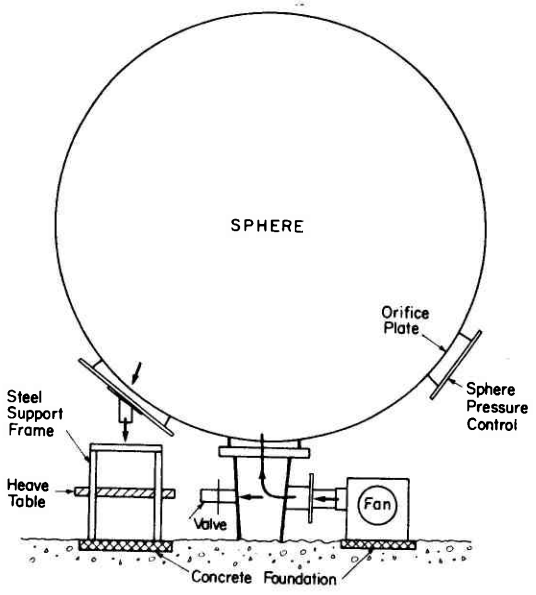
$$\omega_h = \sqrt{\frac{a^2}{L_d V_{ce}} A_d}, \qquad f_h = \frac{\omega_h}{2\pi} \qquad (21)$$

To verify the predictions, a number of experiments were devised. The initial series used the UTIAS heave table facility. A centrifugal fan situated on the roof of the building forced air through a 0.3m diameter 6.1m long supply duct to a 2.5m^3 tank. The stability experiments, which were situated directly below the tank, received air from it through a relatively short flexible duct. The tank had been installed in an earlier experiment in an attempt to make the air feed system behave like a constant pressure source. With the constant pressure assumption, the theory predicted that at a given cushion pressure, p_{ce}, the system would become unstable as h_e/D_p was increased. The exact opposite was found experimentally. Calculations based on an acoustic model of the 6.1m long feed duct indicated that the size of the tank would have to be increased by a factor of several hundred in order to satisfactorily approximate a constant pressure source. It was impossible to modify the original experiment in this way. Fortunately, the author had access to a 950m^3 hollow sphere and a special experiment was built around it as shown in Figure 4. Its dimensions are given in Table 2. A standard industrial fan supplied pressurized air to the sphere, and the sphere, which acted as a pneumatic filter, in turn supplied air to the test duct and tapered cell cushion. The air flow rate through the cushion was controlled by bypassing some air directly to atmosphere through exhaust ports. The cushion was constrained by a linear recirculating ball bearing assembly to move vertically in heave only over a rigid flat table. It was coupled to the test duct by a short length of flexible ducting. The test duct was fixed in the inertial reference frame. The H beam support structure was bolted to a concrete foundation. A conical inlet, calibrated in situ by an ASME standard orifice plate, was used to measure the equilibrium cushion flow. A detachable baffle plate, mounted on the table below the inlet to the cushion, was used in an attempt to minimize internal flow effects. Two skirts were used, one rigid and one flexible. The lip discharge coefficient for each was measured experimentally after the cushion was installed.

A typical result showing a duct effect is given in Figure 5. The duct length was 1.71m and the skirt was rigid. The theoretical results for both isothermal and isentropic cushion thermodynamic processes are given. The agreement between the isentropic boundary and the experiments can be seen to be excellent. Thus, for the sphere facility duct-plenum model, the use of the lumped capacitance cushion model with all its inherent assumptions is justified. Figure 6 compares the stability boundaries obtained experimentally for the rigid skirt and the flexible skirt. The effect of flexibility can be seen to be very small. Figure 7 compares theory and experiment for a duct length of 3.26m, where the data in Figure 6 was used to determine an equivalent static stiffness coefficient for the flexible skirt.

3.2 Internal Flow Effects

It is clear that if the equilibrium flow is increased sufficiently, internal flow structure can be made to have a significant effect. Typically, for the model used in the sphere experiments, the cushion may begin to act as if it is a jet directed vertically downward against the ground



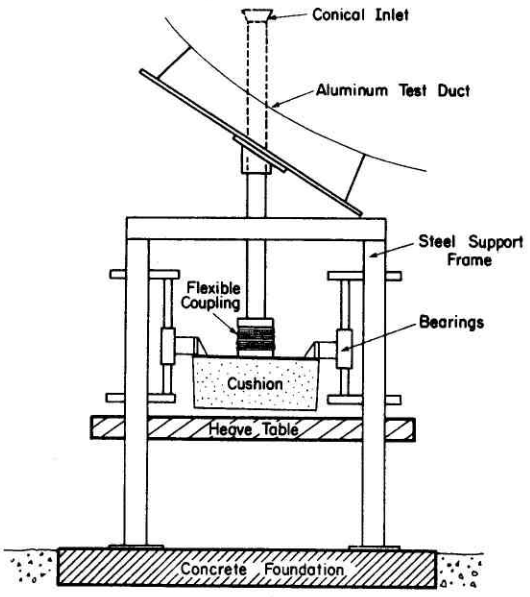


Fig. 4 Sphere facility

Dimensions of sphere facility

Sphere diameter		=	12.2m (40 ft)
Skirt diameter	top	=	0.508m (1.67 ft)
	bottom	=	0.467m (1.53 ft)
Skirt height		=	0.213m (0.70 ft)
Duct length	long	=	3.26m (10.7 ft)
	short	=	1.71m (5.6 ft)
Duct diameter		=	0.0779m (0.256 ft)
Basic model weight	flexible	=	49.35N (11.09 lbs)
	rigid	=	58.96N (13.25 lbs)
Duct flow friction factor		=	0.01656
Lip discharge coefficient	flexible	=	0.567
	rigid	=	0.60

Duct discharges directly into the cushion.

Skirts for sphere experiment

Flexible skirt:		
Material	=	Uniroyal Fiberthin 131 (rubber coated fabric)
Thickness	≅	0.51 mm
Weight	=	6.97 Pa
Rigid skirt:		
Material	=	Aluminum
Thickness	≅	1.25 mm

Table 2

board. To study this phenomena steady state flow structures were obtained by finite difference numerical computation applied to the partial differential equations used for modelling recirculating turbulent flows. The numerical technique was that developed by Gosman and Ideriah[8] for the primitive variable (u, v, p) Navier-Stokes formulation with an eddy viscosity (k-ε) turbulence model.

Figures 8 and 9 give typical velocity vector diagrams obtained for one cell from a multicell air cushion. These suggest one way in which the internal flow structure might affect cushion dynamics. For high enough flow rates, the dynamic head of the radial wall jet near the cushion exit would be comparable to the cushion pressure. This means that the lip orifice flow equation would become

$$Q_a = C_{da} \ell h \sqrt{\left(\frac{2p_c}{\rho} + V_{jet}^2 \right)} \qquad (22)$$

$$V_{jet} = k_{jet} \frac{Q_d}{A_d}$$

where C_{da} would be significantly higher than the classical value of 0.61. Stability boundaries for the case where the radial wall jet was assumed to respond quasi-statically to the duct flow are shown in Figure 10 for the sphere facility duct-plenum model. These are in good qualitative agreement with results obtained experimentally (Figure 11). It is to be expected that the effect would be small for platform air cushions, having planform dimensions much larger than the skirt

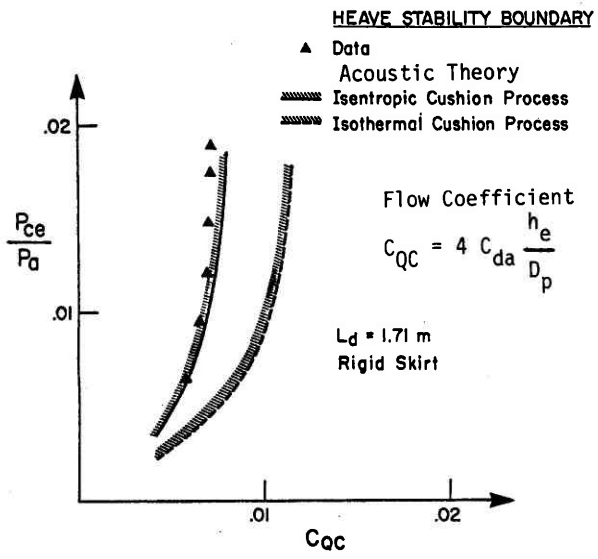


Fig. 5 Typical comparison of theory and sphere facility experiment showing duct effect

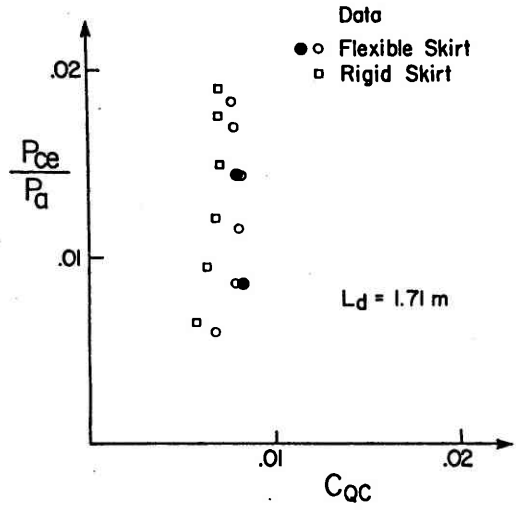


Fig. 6 Comparison of rigid skirt and flexible skirt data

height, because, if the supply is located centrally, the radial wall jet would be dissipated by the action of viscosity before it could reach the cushion exit.

3.3 Nonlinear Effects

A nonlinear analysis provides insights into the practical importance of linear predictions. For example, it is conceivable that a nonlinear system which is unstable in a linear sense could be practically stable because it could enter a limited amplitude oscillation or limit cycle which is of sufficiently small amplitude that the basic operation of the system is not adversely affected. Similarly, a nonlinear system which is stable in

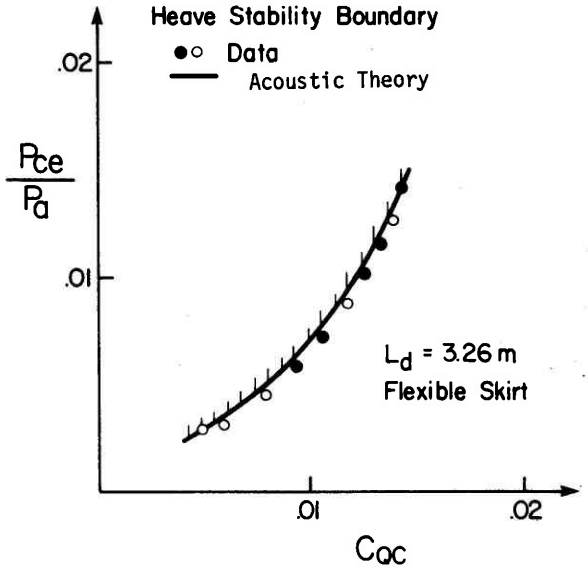


Fig. 7 Long duct comparison

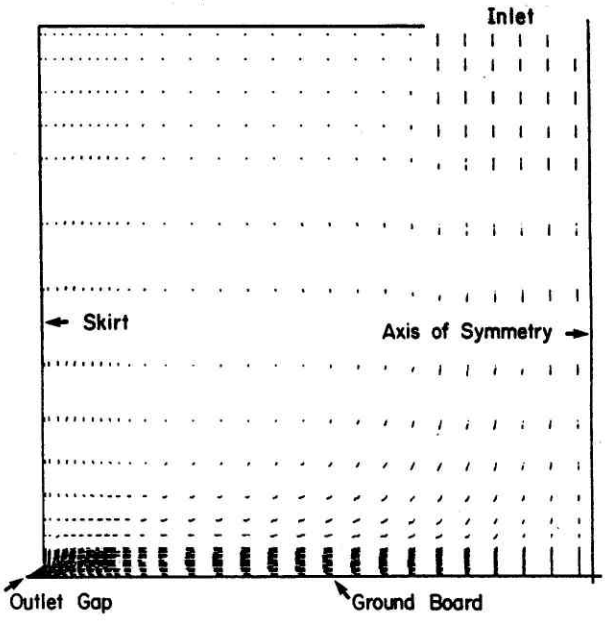


Fig. 8 Velocity vector plot for single cell cushion. Inlet Re=10^4

a linear sense could be practically unstable.

Nonlinearities in air cushion systems can arise from several sources. For example, the source of cushion air often has a nonlinear static pressure-flow characteristic, as discussed earlier. The compression expansion process in the cushion volume itself is governed by a polytropic equation of state. This would contribute significant nonlinear effects if the pressure oscillations are large compared to atmospheric

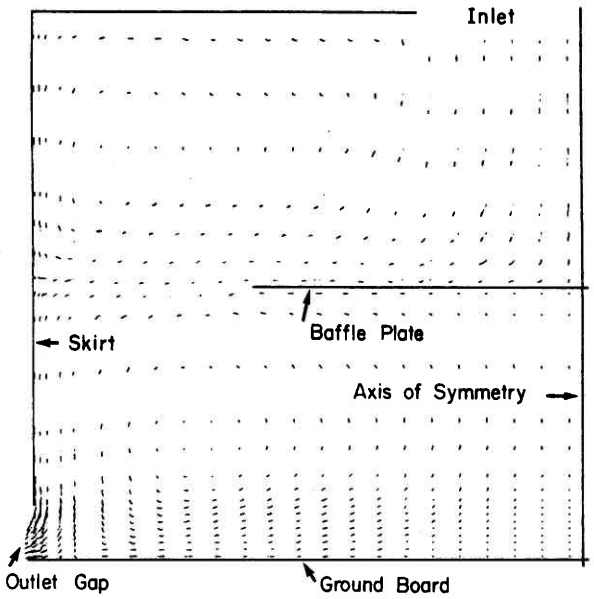


Fig. 9 Velocity vector plot for single cell cushion with baffle plate. Inlet Re=10^5

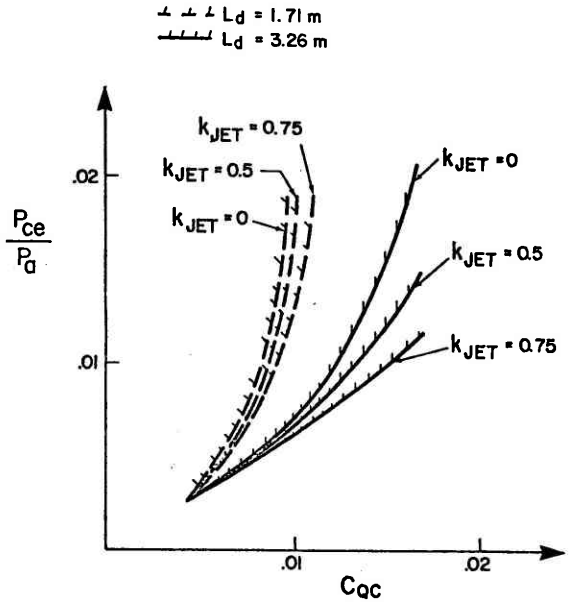


Fig. 10 Internal flow effect on heave stability: theory

pressure. The unsteady air escape from the cushion to atmosphere is assumed quasi-static and is thus modelled by the one dimensional orifice flow law. This has two associated nonlinearities. One is the square-root dependence of the volume flux on the cushion pressure coupled to a varying leakage area. The second is characteristic of vehicles equipped with flexible skirts and this is shut-off associated with skirt-ground contact. Finally, it is

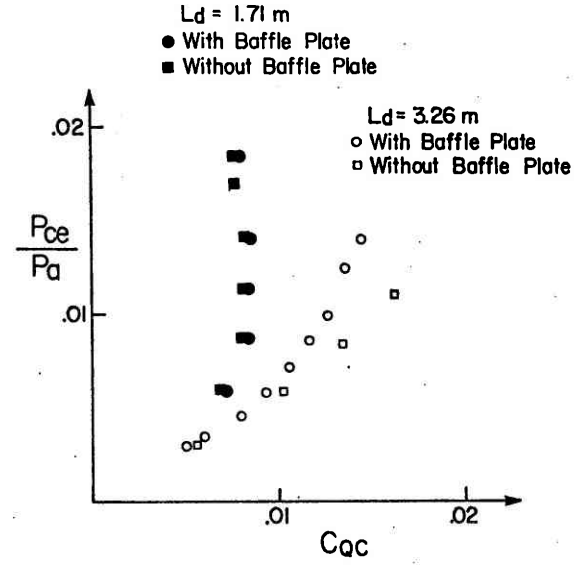


Fig. 11 Internal flow effect on heave stability: sphere facility experiment

known that under certain circumstances the static heave, pitch and roll stiffness characteristics of flexible skirted cushions can display significant hysteretic behaviour.

In the work at UTIAS attention has been restricted to the two nonlinearities that seem universally characteristic of air cushions; these are the Bernoulli law for orifice flows and shut-off. Amplitude and frequency results obtained from a Galerkin describing function analysis of limit cycles in a duct-plenum system were found to agree closely with those of a Runge-Kutta numerical simulation. The details of the Galerkin analysis are given in reference 9. For it, one assumes solutions of the form

$$\phi_i \cong \phi_{ib} + \sum_{n=1}^{N} \phi_{in}^{s} \sin n\omega t + \sum_{m=1}^{M} \phi_{im}^{c} \cos m\omega t \quad (23)$$

where ϕ_i would be typically $(h, p_c, Q_d \ldots)$. When these solutions are substituted into the governing nonlinear ordinary differential equations, one obtains the generally nonzero residuals $R_j(\phi_i)$. The Galerkin technique forces these residuals to be zero in a weighted average sense by making them orthogonal to weighting functions as shown below

$$\int_0^{2\pi/\omega} W_k R_j(\phi_{ib}, \phi_{in}^{s}, \phi_{im}^{c}, \omega, t)dt = 0 \quad (24)$$

where the weighting functions W_k are taken to be 1, sin $n\omega t$, cos $m\omega t$. The integrations give a set of nonlinear algebraic equations for the coefficients ϕ_{ib} ϕ_{in}^{s} ϕ_{im}^{c} and for the frequency ω. Both the numerical simulations and the Galerkin technique showed that the motion on the unstable side of linear stability boundaries is usually a limit cycle. The limit cycle amplitude is usually such

that the system can be described as practically unstable. It was also shown how one might suppress limit cycles by injecting a high frequency or 'dither'[10,11] pressure oscillation into the system nonlinearities. However, this idea needs to be confirmed experimentally because the quasi-static orifice flow law might be inadequate at such high frequencies.

4. UTIAS: RECENT WORK

4.1 Limit Cycle Experiment

Limit cycle amplitudes and frequencies were measured using the sphere facility duct-plenum model. Comparisons with the numerical results of simulations based on acoustic and lumped inertance duct models showed good qualitative agreement. Two locally stable limit cycles were found to exist; one high frequency low amplitude mode and one low frequency high amplitude mode. Pressure waveforms, both measured and calculated, were found to exhibit higher harmonics. Typical examples are shown in Figures 12 and 13. This work is described in detail in reference 12.

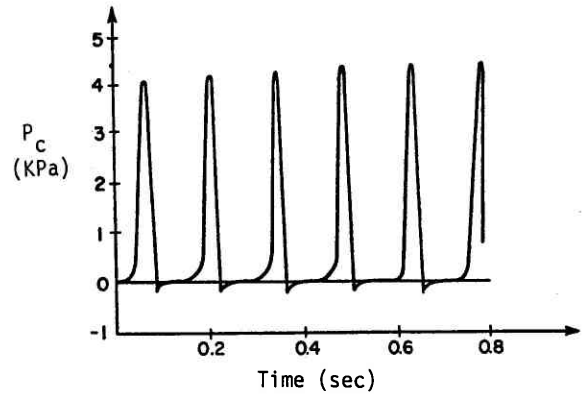


Fig. 12 Limit cycle for a duct plenum model: numerical simulation

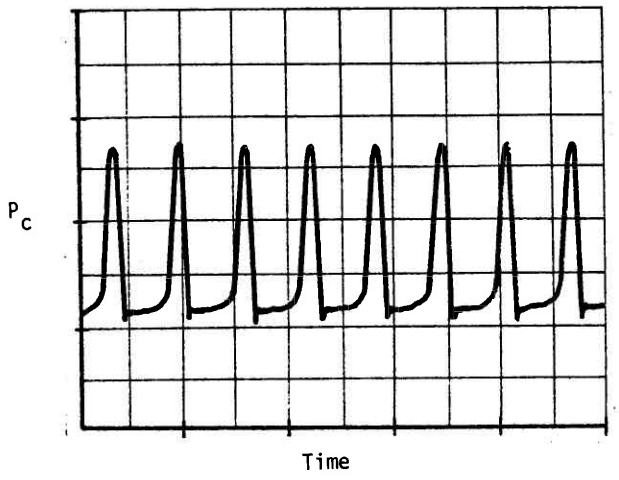


Fig. 13 Limit cycle for a duct plenum model: sphere facility experiment

4.2 Skirt damping

Phenomenological models, based on measured viscoelastic properties of model skirt materials, were incorporated into the theory for the sphere facility duct-plenum model. Typical comparisons of theory and experiment are shown in Figures 14 and 15. As can be seen, the agreement is good for the plastic skirt but not so good for the nylon fabric skirt. Also the stability for the nylon skirt case is pressure history dependent and very sensitive to the effective hoop Poisson's ratio of the skirt ν_{eff}.[13,14] This ratio relates changes in cushion pressure to changes in skirt height and thus leakage flow area. It is not easy to measure experimentally. This is because it is made up of three components. The first is the basic positive ratio associated with hoop extension, the second is a negative contribution due to skirt taper, and the third is a positive contribution due to the curvature at the top of the cell. For the nylon skirt, this effective Poisson's ratio is dominated by the latter. As shown in Figure 15 it could be used to improve stability quite considerably.

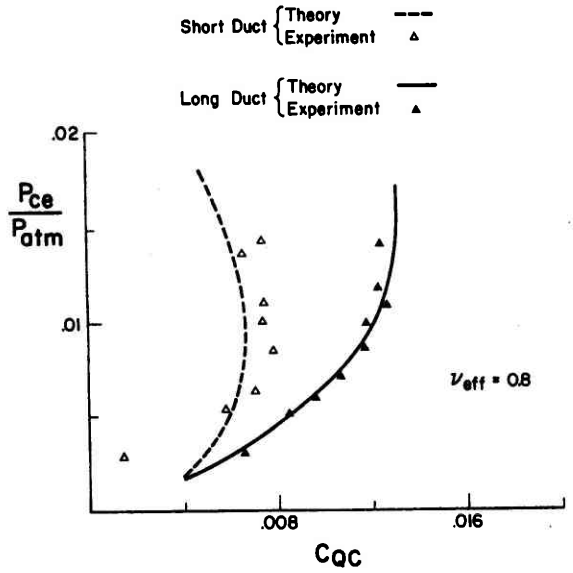


Fig. 14 Comparison of theory and experiment for plastic skirt

4.3 Large Air Cushion Platforms

There are many potential Canadian uses for large air cushion platforms with planform dimensions much larger than the skirt height. However, for such cushions the time required for a pressure wave to travel from one end of the cushion to the other could be of the same order as the time for a typical vehicle oscillation. This implies that the lumped capacitance model would be inadequate because the pressure would not be uniform throughout the cushion at any instant in time. Reference 15 presents some theoretical work for a large geometrically axisymmetric air cushion platform (Figure 16) subjected to axisymmetric disturbances for which the resulting motion is pure heave, the most

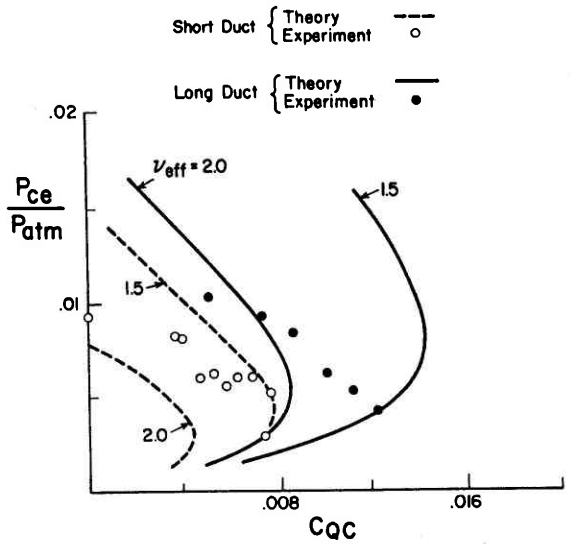


Fig. 15 Comparison of theory and experiment for nylon skirt

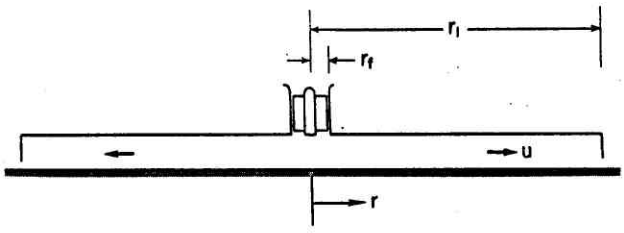


Fig. 16 Large axisymmetric air cushion platform

often observed motion. Non-axisymmetric disturbances which would also excite pitch as well as heave are not considered. The results obtained show that significant destabilizing wave effects can occur at low cushion pressures. Also, the frequency of heave oscillation was found to be given approximately by

$$\omega_p = \sqrt{\frac{\rho a^2}{h_s}\frac{g}{p_{ce}}} \qquad f = \frac{\omega_p}{2\pi} \tag{25}$$

where the parameters are as given earlier. This formula can be derived by ignoring the flow into and out of the cushion; it is simply the frequency of a mass on an air spring. It suggests that for a given geometry wave effects would be excited mainly at low cushion pressures. A frequency calculation for the large Canadian air cushion, the ACT-100 (20m by 15m), based on the above equation gives approximately 2 Hz. This is for a cushion pressure of 6.5 KPa and a skirt height of 1.5m. The frequency observed during field trials is of this order.

4.4 Air Cushion Landing Gear Trunk Flutter

One problem encountered by developers of air cushion landing gear is trunk flutter. Most studies of this conclude that the instability is inherently nonlinear and that it is due to a static divergence of the trunk caused when the negative stiffness associated with the airflow under the trunk becomes in an absolute value sense greater than the positive stiffness associated primarily with trunk tension. UTIAS work, reported recently in reference 16, shows that the flutter is not necessarily a nonlinear phenomena. A Kelvin-Helmholtz type linear stability analysis similar to that used for aeroelastic problems such as panel flutter was used and it predicted a divergent oscillation at about the conditions for which flutter was observed in a prototype system.

4.5 Stability Over Water

Fowler[17] recently showed experimentally that significant destabilizing effects can occur when operating air cushions over water. His experiments on the small Canadian research craft known as HEX-5 showed that 'overland the vehicle would not self-oscillate at any point in its operating range whereas over water it showed heave oscillation clearly and systematically.'[17]

The UTIAS work on stability over water, described in detail in references 18 and 19, was motivated by this experimental result. In reference 18, two-dimensional linearized water wave theory[20-22] was used to study the effects of cushion volume modulation and lip air flow modulation resulting from water surface motion. For the averaged piston-like motion of the water surface directly beneath the vehicle, the water wave theory gave (Appendix)

$$\frac{\overline{\Delta\eta}(i\omega)}{\Delta p(i\omega)} = N(i\omega) = A + Bi \tag{26}$$

while for the water surface motion at the lip it gave (Appendix)

$$\frac{\Delta\eta_{lip}(i\omega)}{\Delta p(i\omega)} = M(i\omega) = X + Yi \tag{27}$$

The lumped capacitance model was used for the air cushion cavity. Flow rates into and out of the cavity were assumed to be governed by the quasi-static orifice flow law

$$Q = C_d A \sqrt{\frac{2p_o}{\rho_a}} \tag{28}$$

Newton's second law was used for the heave displacement of the vehicle. It was assumed that the response functions $N(i\omega)$ and $M(i\omega)$ were not affected by transients in the basic air cushion suspension. This gave the following characteristic equation with complex coefficients

$$C_o s^3 + C_1 s^2 + C_2 s + C_3 = 0 \tag{29}$$

where

$$C_o = \frac{h_s m}{\rho a^2} - N(i\omega)m$$

$$C_1 = \left[\frac{Q_e}{2(p_{fe} - p_{ce}) - C_{PQ}Q_e} + \frac{Q_e}{2p_{ce}}\right]\frac{m}{2b}$$

$$- \frac{Q_e}{h_e} M(i\omega) \frac{m}{2b} \qquad (30)$$

$$C_2 = 2b, \qquad C_3 = \frac{Q_e}{h_e}$$

When critical stability occurs, $s = i\omega$.[4,24] In this case, the characteristic equation reduces to

$$\Delta R + \Delta I i = 0 \qquad (31)$$

which gives the two conditions

$$\Delta R = 0, \qquad \Delta I = 0 \qquad (32)$$

When h_e is specified, the two remaining unknowns in the ΔR and ΔI conditions are p_{ce} and ω. These can be found most easily using a graphical technique based on the Nyquist block diagram representation shown in Figure 17. When $s = i\omega$, the curve $G(i\omega)$ $H(i\omega)$ passes through the minus-one point in its complex plane as ω is varying from 0 to ∞ where

$$G(i\omega) = \frac{-\frac{Q_e}{h_e} - 2bi\omega}{C_c i\omega + \left[\frac{Q_e}{2(p_f - p_{ce}) - C_{PQ}Q_e} + \frac{Q_e}{2p_{ce}}\right] - \frac{Q_e}{h_e}(X+Yi) - 2bi\omega(A+Bi)} \qquad (33)$$

$$H(i\omega) = \frac{2b}{m\omega^2}$$

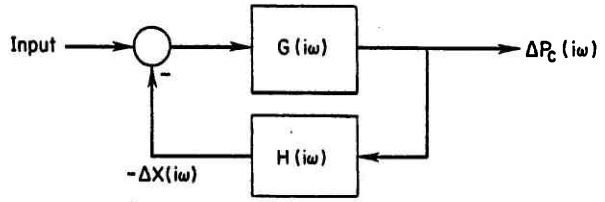


Fig. 17 Nyquist block diagram for over-water stability

When the phase angle of $G(i\omega)$ $H(i\omega)$ is less negative than -180° when $|G(i\omega)\ H(i\omega)|$ is equal to 1, the force acting on the suspension mass leads the negative of the heave motion whereas when the phase is more negative than -180° the force lags. Simple arguments based on the work done on the suspension mass during an oscillation cycle show that the lead case is stable while the lag case is unstable.

The theory was applied to the HEX-5 craft mentioned earlier (Table 3). For the typical operating gap, h_e = 4.57 mm, rigid surface calculations based

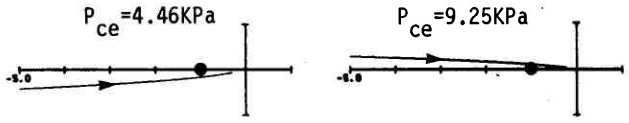
	Assumed orifice flow discharge coefficients
Length = 3.75m	Fan = 0.61
Width = 2.5m	Lip = 0.80
Depth = 0.2m	

The fan is modelled as an orifice between the cushion and a constant pressure source. The size of the orifice is based on the following fan slope per meter length of vehicle

$$\left.\frac{dp_c}{dQ}\right|_e = -1.875 \frac{\text{KPa}}{\text{m}^3/\text{sec}} \text{ at } p_c = 1 \text{ KPa}$$

Table 3 HEX-5 data

on the Routh Hurwitz criteria indicated that the system would be unstable above p_{ce} = 6.84 KPa and stable below. Thus, over land HEX-5 should be very stable because typical operating pressures are of the order of 1 KPa. The above theory gives for the rigid surface case the plots shown in Figure 18. These show that the critical stability pressure lies approximately midway between 4.46 KPa and 9.25 KPa. Typical plots for the volume modulation acting alone are shown in Figure 19. These show a large increase in critical stability pressure relative to overland. Typical plots for volume modulation and flow modulation acting together are shown in Figure 20. These show unstable behaviour at low cushion pressures. Other plots obtained show that when flow modulation and volume modulation are acting together flow modulation dominates. The quoted references give a discussion of these results.



Imaginary - Vertical Scale

Real - Horizontal Scale

Fig. 18 Nyquist plots for rigid surface case

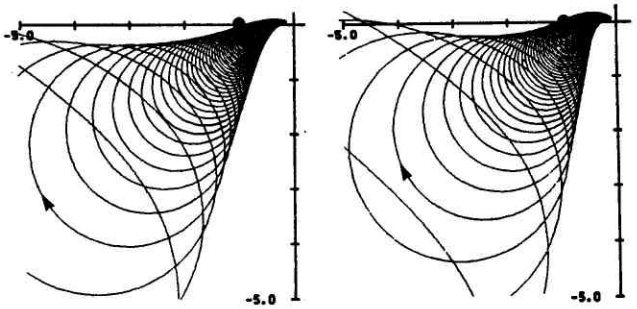


Fig. 19 Nyquist plots showing volume modulation effect

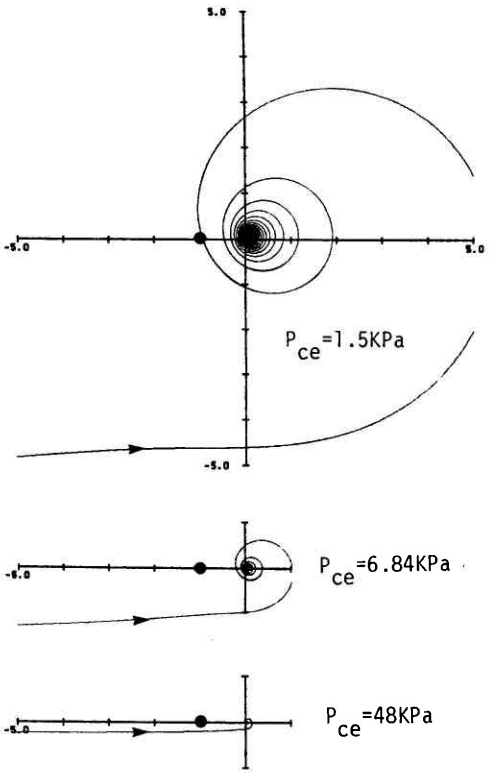


Fig. 20 Nyquist plots showing flow modulation effect

Thus it appears that the instabilities observed by Fowler[17] were caused mainly by lip air flow modulation. However, when the lip air flow for HEX-5 was studied separately by mounting three segments from its segment skirt in a small water tank, another type of instability was observed. For certain air flow rates the air flow directly beneath the segments interacted with the water-free surface and caused it to become unstable. In extreme cases the water surface was sucked upward until contact with the segments occurred. The cavity pressure would then build up forcing open a channel through which the air could again flow. The above repeated itself at a frequency of about 5 Hz. This is close to the heave oscillation frequency of 4.6 Hz measured by Fowler.[17]

5. UTIAS: WORK IN PROGRESS

5.1 Unsteady Orifice Flow

A finite element numerical simulation applied to the equations governing unsteady orifice flow is being used to determine the range of validity of the quasi-static orifice flow law. The aim is to compare the $\partial V_s/\partial t$ term to the $V_s(\partial V_s/\partial s)$ term in

$$\underbrace{\frac{\partial V_s}{\partial t}}_{\text{local acceleration}} + \underbrace{V_s \frac{\partial V_s}{\partial s}}_{\text{convective acceleration}} + \frac{1}{\rho}\frac{\partial p}{\partial s} = 0 \qquad (34)$$

for typical geometries and frequencies of interest. Simple order of magnitude arguments give

$$\frac{\Delta\left(\frac{\partial V_s}{\partial t}\right)}{\Delta\left(V_s \frac{\partial V_s}{\partial s}\right)} \cong \alpha \frac{L_o \omega}{V_{oe}} \qquad (35)$$

where α is of the order of unity, L_o is the characteristic length of the orifice, ω is the oscillation frequency, and V_{oe} is the flow velocity at the vena-contracta. Note that if V_{oe} tends to zero, the local term dominates.

5.2 Unsteady Fan Characteristics

The unsteady pressure-flow characteristics of various air cushion fans are being measured experimentally and the data is being compared to theories such as that proposed by Ohashi.[25] An oscillating ground board is used to provide a sinusoidally varying leakage area in time. The ground board motion and the corresponding cushion pressure variation are measured and the lumped capacitance equation for the cushion is used to obtain

$$Q_c = C_c \frac{dp_c}{dt} + C_{da} \ell h \sqrt{\frac{2p_c}{\rho}} + S \frac{dh}{dt} \qquad (36)$$

The fan characteristic is just a plot of Q_c versus P_c.

The theory proposed by Ohashi accounts for unsteady blade aerodynamics and to first order gives

$$\frac{\Delta p_f(s)}{\Delta Q_f(s)} \cong \frac{C_{PQ}}{\tau_c s + 1} \qquad (37)$$

where

$$\tau_c = \frac{1}{\alpha} \frac{\cos \lambda_R}{2\pi N_R \phi n} \qquad (38)$$

$$\phi = \frac{\text{exit flow velocity}}{\text{rotor tip velocity}} \qquad (39)$$

where

$$\begin{aligned} N_R &= \text{number of rotor blades} \\ n &= \text{fan speed (rps)} \\ \lambda_R &= \text{stagger angle} \\ \phi &= \text{flow coefficient} \\ \alpha &= 0.3 \text{ theoretically} \\ &= 0.1 \text{ experimentally} \end{aligned} \qquad (40)$$

One can see from the above equations how unsteady aerodynamics could be important. If τ_c is very large relative to the period of a typical vehicle oscillation, then the fan would tend to behave as a constant pressure source. Note that τ_c is directly proportional to the time taken for a typical air particle to travel one blade chord length.

5.3 Large Rectangular Air Cushion Platforms

The work on large air cushion platforms is being extended to include rectangular geometries.

6. CONCLUSIONS

Although the lumped capacitance model has a number of limitations, it does provide important insights and it suggests a number of stabilization techniques. A major feature of the work at UTIAS has been the use of a large hollow sphere to isolate the test cushion from fan dynamics. To date the effects of supply ducts, cushion volume internal flows, skirt damping and nonlinear or limit cycle phenomena have been studied using this facility. It will soon be used to test out a number of stabilization techniques suggested by theory. Some theoretical work has also been done on stability over water and on stability of large air cushion platforms.

ACKNOWLEDGEMENT

The funding for this work, provided by the National Research Council of Canada and by the Canadian Transportation Development Centre, is gratefully acknowledged. The support received from my supervisor and colleague, Dr. P. A. Sullivan, is also sincerely appreciated.

REFERENCES

1. Tulin, M. P., 'On the Vertical Motions of Edge Jet Vehicles', Symposium of Ground Effect Phenomena, Princeton University, N.J., Oct. 1959.

2. Ribich, W. A., and Richardson, H. H., 'Dynamic Analysis of Heave Motion for a Transport Vehicle Fluid Suspension', Dept. of Mechanical Engineering, MIT, 1967, Report DSR-76110-3.

3. Hughes, P. C., 'Lecture Notes on the Stability of Ordinary Differential Equations', UTIAS, 1976.

4. Hahn, W., 'Stability of Motion', Springer-Verlag, 1967.

5. Hinchey, M. J., 'Heave Instabilities of Amphibious Air Cushion Suspension Systems', Ph.D. Thesis, UTIAS Report No. 246, Nov. 1980.

6. Hinchey, M. J., and Sullivan, P. A., 'Duct Effects on the Heave Stability of Plenum Air Cushions', Journal of Sound & Vibration, 60, 1, 1978, pp. 87-99.

7. Sullivan, P. A., Hinchey, M. J., and Green, G. M., 'Prediction and Measurement of Dynamic Stability Boundaries of Plenum Air Cushions', Journal of Sound & Vibration, Sept. 1982.

8. Gosman, A., and Ideriah, F., 'Teach-T: A General Computer Program for Two Dimensional, Turbulent Recirculating Flows', Dept. of Mechanical Engineering, Imperial College, London, 1976.

9. Hinchey, M. J., and Sullivan, P. A., 'A Theoretical Study of Limit Cycle Oscillations of Plenum Air Cushions', Journal of Sound & Vibration, 79, 1, 1981.

10. Oldenburger, R., and Makada, T., 'Signal Stabilization of Self-Oscillating Systems', Institute of Radio Engineers Transactions on Automatic Control, AC6,319-325, 1961.

11. Oldenburger, R., and Boyer, R. C., 'Effects of Extra Sinusoidal Inputs to Nonlinear Systems', Journal of Basic Engineering, 84, 1962, pp. 559-570.

12. Sullivan, P. A., Byrne, J. E., and Hinchey, M. J., 'Limit Cycle Theory and Experiment for a Duct-Plenum System', Submitted to the Journal of Sound & Vibration.

13. Graham, T. A., 'The Effect of Skirt Material Choice on the Heave Stability of a Duct-Plenum Air Cushion', Master's Thesis, UTIAS, 1980.

14. Graham, T. A., Sullivan, P. A., and Hinchey, M. J., 'Skirt Material Effects on the Heave Stability of a Duct-Plenum Air Cushion', Submitted to the ASME Journal of Applied Mechanics.

15. Hinchey, M. J., Sullivan, P. A., and Dupuis, A., 'On the Heave Dynamics of Large Air Cushion Platforms', UTIAS TN 234, Submitted to the Journal of Sound & Vibration.

16. Hinchey, M. J., and Sullivan, P. A., 'Kelvin-Helmholtz Stability Analysis of Air Cushion Landing Gear Trunk Flutter', Journal of Aircraft (AIAA), Vol. 19, No. 1, 1982.

17. Fowler, H., 'An Experiment on the Heave Oscillation of a Light Air Cushion Vehicle Over Water', Canadian Aeronautics & Space Journal, Vol. 2, No. 2, Second Quarter 1980.

18. Hinchey, M. J., 'Heave Stability of Air Cushions Hovering Over Deep Water', UTIAS TN 236, Submitted to the Journal of Fluid Mechanics.

19. Hinchey, M. J., and Sullivan, P. A., 'Kelvin-Helmholtz Instabilities in Air Cushions Hovering Over Water', Submitted to the Journal of Fluid Mechanics.

20. Ogilvie, T. F., 'Oscillatory Pressure Fields on a Free Surface', Dept. of Naval Architecture and Marine Engineering, College of Engineering, University of Michigan, Sept. 1969.

21. Stoker, J. J., 'Water Waves - The Mathematical Theory with Applications', Interscience Publishers, Pure and Applied Mathematics Series, Vol. IV, 1957.

22. Lamb, H., 'On Deep Water Waves', Proceedings of the London Mathematical Society, Series 2, Vol. 2, 1904.

23. Abramowitz, M., and Stegun, I., 'Handbook of Mathematical Functions with Formulas, Graphs, and Mathematical Tables', Dover Publications, 1972.

24. Fung, Y. C., 'An Introduction to the Theory of Aeroelasticity', Dover Publications, 1969.

25. Ohashi, H., 'Analytical and Experimental Study of Dynamic Characteristics of Turbopumps', NASA TN D-4298, April 1968.

APPENDIX

The pressure-water surface interaction transfer functions according to Lamb are:

Spatially averaged water surface motion

$$A = \frac{2}{\rho_w g \nu b} [\kappa - \sin\nu b \cos\nu b] \tag{41}$$

$$B = \frac{2}{\rho_w g \nu b} \sin^2 \nu b \tag{42}$$

Water surface motion at lip

$$X = -\frac{1}{\pi \rho_w g} [4\pi - \psi - 4\pi \sin^2 \nu b] \tag{43}$$

$$Y = \frac{4}{\rho_w g} \sin\nu b \cos\nu b \tag{44}$$

where

$$\nu = \frac{\omega^2}{g} \tag{45}$$

and

$$\kappa = \frac{\nu^2}{\pi} \int_0^\infty \frac{e^{-mb} \sinh mb}{m(m^2+\nu^2)} dm \tag{46}$$

$$\psi = 4\nu \int_0^\infty \frac{e^{-mb} \cosh mb}{m^2+\nu^2} dm \tag{47}$$

COMPUTER STUDIES OF ACV HEAVE PERFORMANCE AS A FUNCTION OF VENT VALVE CONTROL PARAMETERS

J.R. Amyot

National Research Council of Canada
Ottawa, Canada

ABSTRACT

A hybrid computer model of the heave dynamics of an air cushion with a segmented skirt and an automatic vent valve control system was used to investigate the effects of control gain and valve set point variations on the hull's response to step changes in ground level. Results have shown that there is an optimum value of control gain and the valve set point position can be set to zero to minimize flow power requirements without significantly changing the dynamical performance.

INTRODUCTION

The use of vent valve control was introduced qualitatively by Fee and Handler[1] in connection with the U.S. Navy's SES-100 surface effect ship and then by Mantle[2] who gave some quantitative ride quality results without elaborating on control strategies. Those results were for operation over water where skirt wear is not as severe as on land and fan speed was not increased to maintain elevation when vent valve set point positions were nonzero. Therefore the observed improvements in ride quality were due not only to vent valve control but also operation at a lower elevation which is itself stabilizing.

Amyot established a method of modeling heave dynamics using fan and skirt characteristic data directly in a synchronous hybrid computer model[3] and then used the method to initiate a computer study of vent valve control in which the elevation was maintained by adjusting fan speed to compensate for a given nonzero vent valve position[4]. The results were very encouraging, especially from the damping standpoint, even though no attempt had been made to optimize the control gain and vent valve set point for best damping and minimum flow power.

Using a slightly modified version of the computer model of Reference 4, this paper probes further into the effects of control gain and valve set point variations on the hull's response to step changes in ground level.

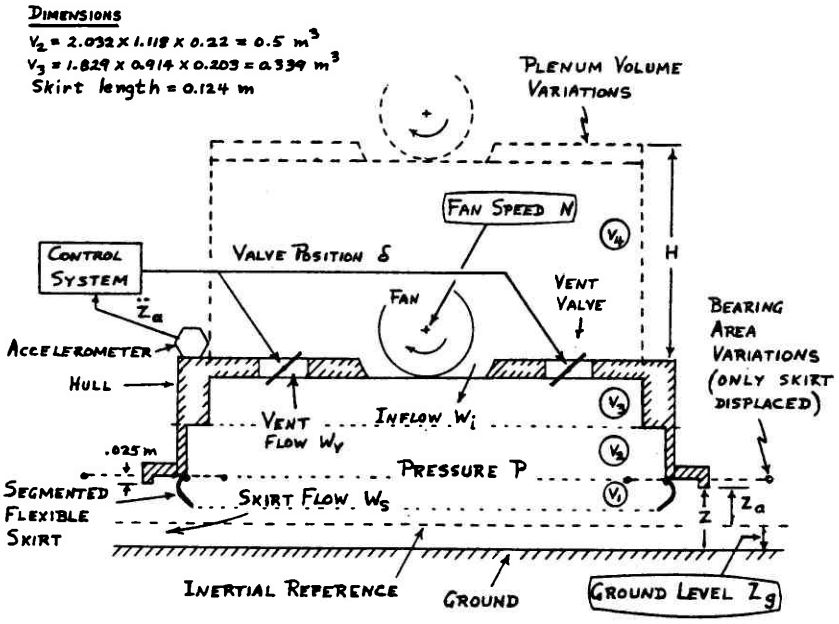


FIG. 1: Schematic diagram

CONCEPTUAL MODEL

The conceptual model is based on Fig. 1 which shows some of the main variables and dimensions. The reader is referred to the nomenclature for definitions of symbols. The inertial reference frame is fixed in space to serve as reference for platform (hull) dynamics and the variable ground level. The bearing area is variable by displacing the skirt inwards or outwards whereas the fixed portion of cushion volume can be varied by changing plenun depth. Symmetrically located wnet valves are controlled in unison by a control system which tries to reduce velocities in a frequency band including the ACV's natural frequencies but excluding operational elevation-control frequencies. Velocity is determined by integration of an accelerometer's output.

Fan speed N is the control variable which determines airflow W_i into cushion volume V, which is variable depending on hull rise height z. An air mass balance relationship involving inflow W_i, outflow W_0 consisting of skirt flow W_s and vent flow W_v, and volume V establishes cushion pressure P which is equal to the net vehicle weight divided by the footprint area under steady conditions at a constant rise height. Mass variations Δm, externally-applied force F and ground level z_g are possible disturbance variables for test purposes although only the latter was used in this study.

The information flow diagram of Fig. 2 gives an overview of the interaction between the ACV, the control system and the operator. The operator sets the bearing area, cushion volume, vent valve set point and control gain prior to a simulation run; then, during the run, he controls fan speed and the occurrence of ground steps interactively.

A mathematical expression of the conceptual model is given in the information flow diagrams of Figs. 3 and 4 and appendices A and B. With the exception of the cushion volume expressions given in Appendix B and the associated data in Appendix A, the model is similar to that of Reference 4.

A first-order high pass filter makes the control system (Fig. 4) less sensitive to low operating frequencies below break frequency ω_a than to high transient frequencies above ω_a, thereby allowing unwanted high frequency components of velocity to be attenuated by the control system while permitting normal operation of the vehicle. Control action is such as to increase the vent valve opening for undesirable upward velocities and to reduce it when they are downwards. If for instance (Fig. 8b) the ground moves upwards in a step, skirt outflow is reduced, cushion pressure increases and the hull rises with a positive value of velocity z_a resulting in a filtered value z_f, an equal control error ϵ and a desired valve displacement $\Delta\delta_d$ proportional to it by factor Kp. This desired displacement added to the desired nominal positon δ_d^* results in a newly increased desired valve position δ_{d2}. Conditional upon the control system being in activated mode by means of pushbutton P_B, this new desired value is transformed to an actual new valve opening δ within specified limits and through actuator and valve dynamics which are assumed for simplicity to be first-order with a break frequency ω_v higher than frequencies being attenuated.

COMPUTERIZED MODEL

The conceptual model was implemented on an EAI 690 hybrid computer consisting of an EAI PACER 100 minicomputer, two EAI 680 analog consoles and an EAI 693 linkage console for high speed data communication between the analog and

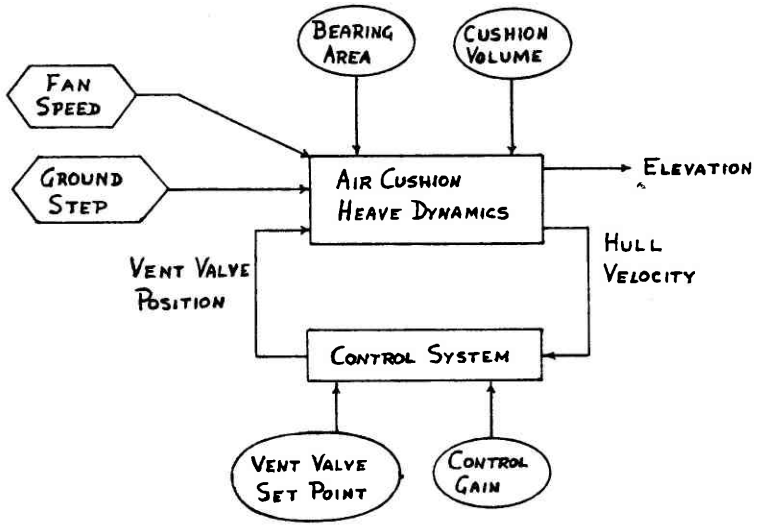


FIG. 2: Overview information flow diagram

digital computers. Analog strip-chart recordings of variables as functions of time were the main form of output. However, specified print-outs were also avaialble by operating a sense switch on the digital console.

The computerized model was operated at one-twentieth of real time for computational stability. It turned out that this was a good time scale factor from a human interaction point of view; therefore, no steps were taken to speed-up the solution.

Parameter values could be changed by operating a sense switch and typing-in new values. Engine speed was controllable continuously by knob from its minimum to maximum value, making it possible to 'operate' the model as one would the physical ACV. Fan speed, applied force, incremental mass and ground-level step tests were available to the operator by pressing pushbuttons.

RESULTS

Two performance parameters were used to determine the influence of control gain K_p and vent valve set point δ^* on heave dynamics. One of these consisted in counting the number of peaks (i.e., positive and negative-going extrema) N_p after which the hull's velocity response to a step change in ground level remained within ± 10% of the magnitude of its first peak. The other was response time T_s at which the hull's elevation returned to and remained within a region defined by its nominal position ± 10% of the disturbance's magnitude. The first criterion was a measure of damping; the second, a measure of the tendency of the skirt to drag and wear during operation over large-scale ground irregularities.

Figures 5 and 6 present N_p and T_s as functions of K_p and δ^* for a ground step downwards of 7.5 cm and specific valve set point positions δ^*=0, 0.1, 0.2 and 0.4. A pronounced reduction in both N_p and T_s is observed for all values of δ^* for increases in the value of K_p from 0 to 3. For all values of δ^* except 0.4, $N_p$and T_s reach minimum values respectively of 2 peaks and 0.6 s in the domain K_p= [3,5]. Beyond this domain, N_p remains constant whereas $T_s$increases to the range [1.2, 1.7] when K_p = 20. The case δ^*= 0.4 is somewhat different in that a minimum value of $T_s \simeq 0.35$ s is obtained for K_p= 8 and three peaks are observed.

It was reported in Reference 4 that flow power is increased by approximately 45% when δ^* is changed from 0% to 40%. Thus, considering the dynamical performance curves of Figures 5 and 6 in conjunction with power requirements, a good choice of control system design parameters would be δ^*=0 and K_p=5.

Time responses for the two cases δ^*=0 and 0.4 with K_p=0 and 5 are shown in Figures 7 and 8. The fan speed was adjusted to give a nominal

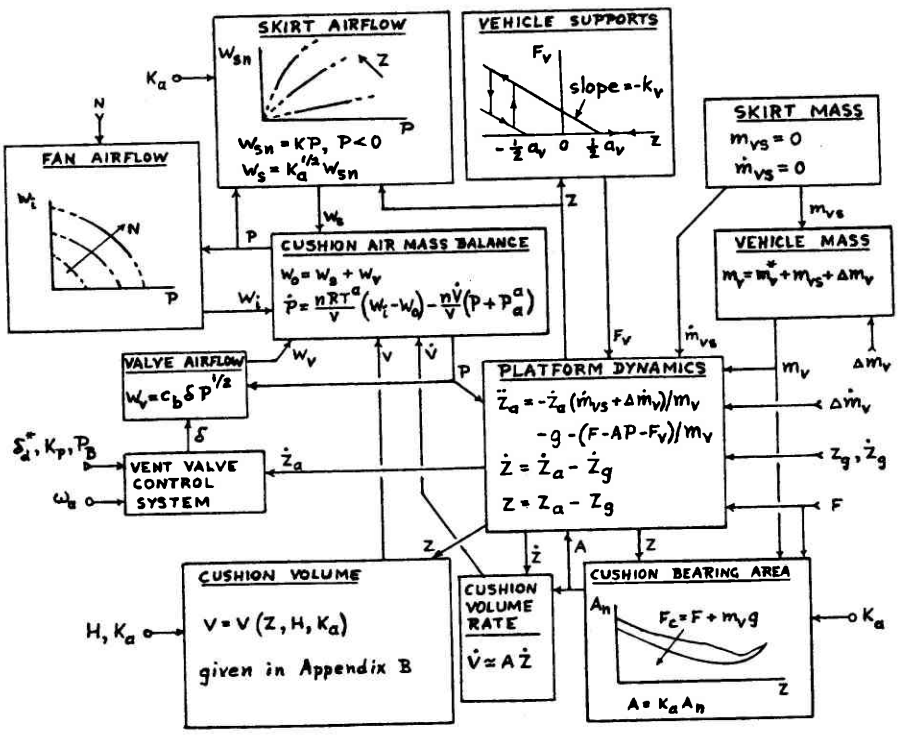


FIG. 3: Air cushion heave dynamics information flow diagram

elevation of 11 cm, i.e., an airgap of 1.1 cm, in each case and ground steps of 7.5 cm amplitude downwards and then upwards were applied. The responses of Figures 7(a) and 8(a), in which K_p=0, are seen to be equally underdamped so that nothing is gained by a fixed opening of vent valves without active feedback control. On the other hand, active feedback control with K_p=5 produces the equally well-damped responses of Figures 7(b) and 8(b). Thus, there is negligible difference in dynamical performance of the platform with δ^*= 0 or 40%. However, the latter vent valve position requires a 45% increase in fan airflow at the same cushion pressure resulting in the same percentage increase in flow power. It follows that a nominal vent valve setting of zero would be advisable to minimize fan power requirements without deteriorating dynamical performance.

CONCLUSION

The effect on platform heave dynamics of varying the vent valve set point from 0 to 40% of its fully-open position was found to be negligible for specific step changes in ground level and large proportional control gain variations in simulation experiments conducted on a computer model. A quasi-optimal value of control gain was

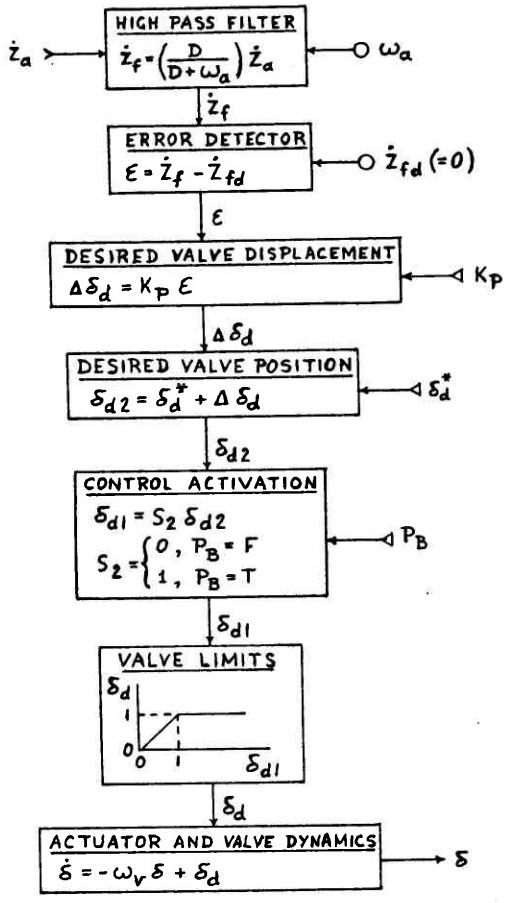


FIG. 4: Control system information flow diagram

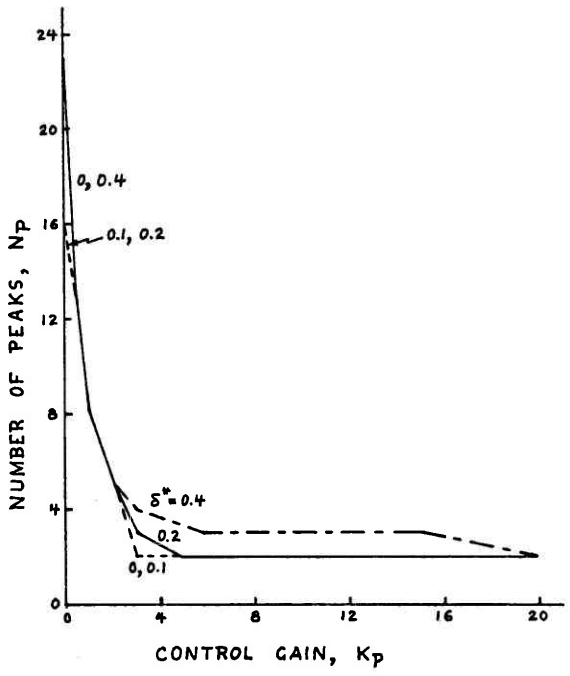


FIG. 5: Number of peaks as a function of control gain and nominal vent valve setting

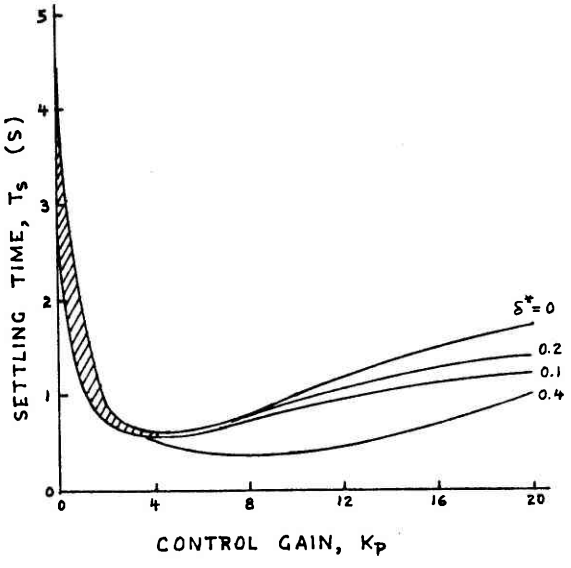


FIG. 6: Settling time as a function of control gain and nominal vent valve setting

found to minimize the number of velocity peaks an elevation settling time following a disturbance.

Since good performance was possible with nominally-closed vent valves, these results strengthen the case for automatic vent valve control of heave dynamics by eliminating the power requirements associated with a non-zero set point position.[4]

A physical model is being constructed at the National Research Council of Canada to validate the analytical work and investigate its practical implications.

NOMENCLATURE

a_v - Vehicle support hysteresis width, m

A - Cushion bearing area, m^2

A_n - Nominal cushion bearing area, m^2

B_0, B_1, B_2 - Parameters in cushion volume equations

B_{0n}, B_{1n}, B_{2n} - Nominal parameters in cushion volume equations

$C_1, \ldots, C_8$ - Parameters in cushion volume equations

F - Vertical applied force, N

F_c - Net vertical force due to weight and applied force, N

F_v - Vehicle support force, N

g - Acceleration due to gravity, m/s/s

K - Proportionality constant in reverse skirt airflow

K_a - factor by which bearing area is increased

k_v - Vehicle support stiffness, N/m

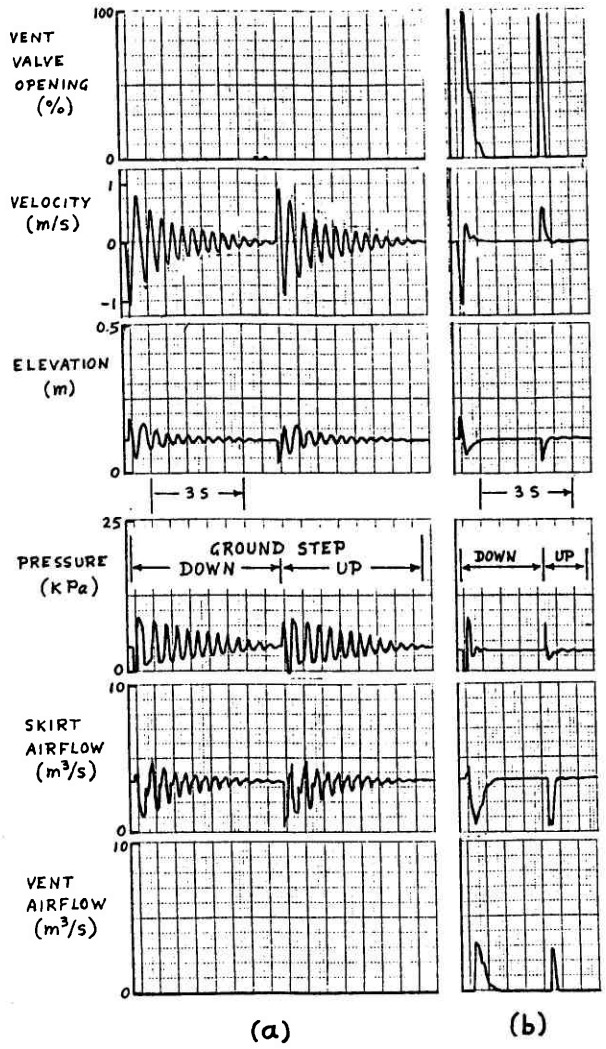


FIG. 7: Time responses to ground step tests; nominal cushion, elevation = 11cm and $\delta^*=0$;(a) $K_p=0$; (b) $k_p=5$

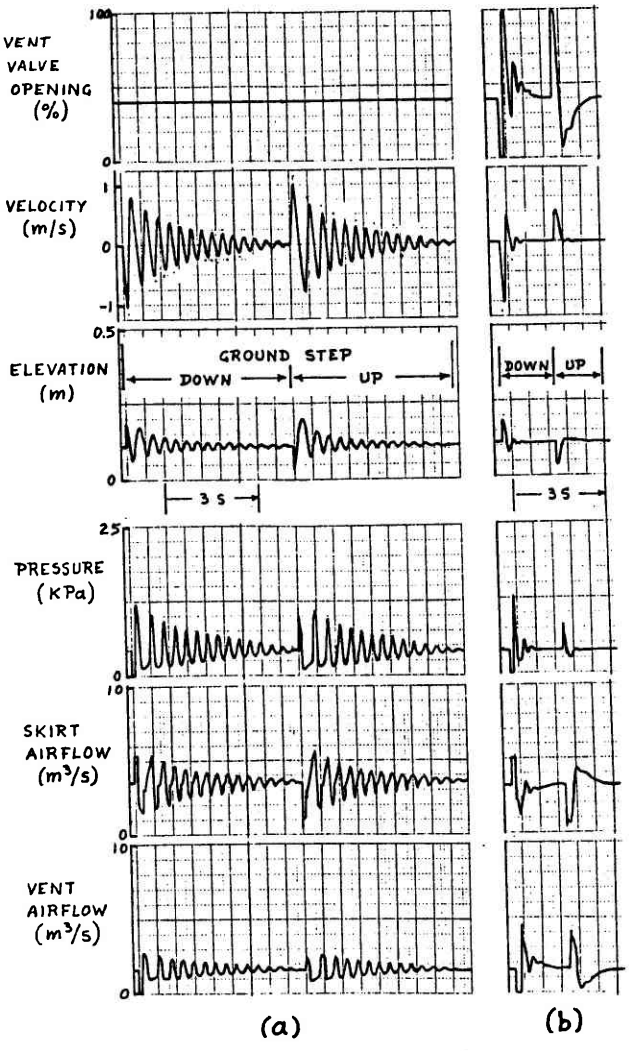


FIG. 8: Time response to ground step tests; nominal cushion, elevation = 11cm and $\delta^*=40\%$;(a) $K_p=0$; (b) $K_p=5$

$L_\perp$ - Height from top of skirt to bottom of support, m

L_s - Fully extended skirt length, m

m_v - Vehicle mass, kg

m_v^* - Vehicle mass without skirt, Kg

Δm_v - Incremental mass added to vehicle, Kg

m_{vs} - Suspended portion of skirt mass, Kg

N - Fan speed, rpm

N_p - Number of peaks in performance measure

n - Polytropic change of state exponent

p - Plenum chamber gauge pressure, Pa

p_a^a - Atmospheric absolute pressure, Pa

P_B - Logical variable determining on-off control system status

R - Universal gas constant, $m^2/(s^2 \cdot K^0)$

S_2 - Internal control system variable

T^a - Plenun absolute air temperature, K°

V - Net cushion volume. m^3

V_F - Parameter in cushion volume equations, m^3

$V_{\perp a}, V_{\perp b}, V_{\perp c}$ -Intermediate cushion volume variables, m^3

W_i - Plenum inlet air flow-rate, kg/s

W_o - Air flow-rate out of plenum, kg/s

z - Distance of supports from ground, m

z_a - Distance of supports from inertia reference, m

$\dot{z}_f$ - Velocity at high-pass filter output, m/s

$\dot{z}_{fd}$ - Desired value of high-frequency velocities, m/s

z_g - Distance of ground from inertia reference, m

$z_\perp$ - Application range limit on cushion volume expressions, m

z_2 - Application range limit in cushion volume expressions, m

α - Parameter in cushion volume equations

δ - Actual vent valve setting

δ_d - Desired vent valve setting

$\delta_{d\perp}, \delta_{d2}$ - Internal control system variables

$\Delta\delta_d$ - Desired valve displacement from nominal setting

ε - Difference between desired and actual high-frequency velocities, m/s

ω_a - High-pass filter break frequency, r/s

ω_v - Actuator and valve break frequency, r/s

A dot over a variable denotes the derivative with respect to time. A superscript asterisk denotes a time-invariant component.

ACKNOWLEDGEMENT

The author is grateful to G. vanBlockand for computer programming assistance.

REFERENCES

1. Fee, J.J., Handler, E.H., 'The U.S. Navy's Large Surface Effect Ship,' Proceedings of the 10'th Canadian Symposium on Air Cushion technology, Ottawa, Canada, 1997.

2. Mantle, P.J., 'Air Cushion Craft Development' Report DTNSRDC-80/012 (4727 Revised), David W. Taylor Naval Ship Research and Development Center, Bethesda, Maryland, January, 1980.

3. Amyot, J.R., 'Computer Model of Heave in Hovercraft HEX-5', Proceedings of the 14'th Canadian Symposium on Air Cushion Technology, Ottawa, Canada, September, 1980.

4. Amyot, J.R., 'Computer Studies of ACV Heave Dynamics Stabilization', Proceedings of the 15'th Canadian Symposium on Air Cushion Technology, Toronto, Canada, September, 1981.

5. Baumeister, T., Avallone, E.A., Baumeister III, T., 'Marks Standard Handbook for Mechanical Engineering', 8th Ed., McGraw-Hill, 1978.

APPENDIX A

Numerical Data

$a_v = 0.0002$ m
$B_{on} = 2.78\ m^2$
$B_{\perp n} = 2.16\ m^2$
$B_{2n} = 2.30\ m^2$
$C_b = 0.066$
$C_\perp = 0.839$
$C_2 = 0.025$
$C_3 = 1.672$
$g = 9.80665\ m/s^2$
$-0.203 \quad H \quad 1.5$ m
$K = 16$ m.s
$0 \quad K_p \quad 10$
$k_v = 6.68 \times 10^6$ N/m

$L_\perp = 0.025$ m
$L_s = 0.124$
$n = 1.396$
$P_a^a = 1.0133 \times 10^5$ Pa
$R = 288.87\ m^2/(s^2 \cdot °K)$
$T^a = 288^0$K
$z_{fd} = 0$ m/s
$z_\perp = 0.10$ m
$z_2 = 0.12$
$562 \quad m_v^* \quad 2346$ kg
$\rho_a = 1.218\ kg/m^3$
$\omega_a = 3.14$ r/s
$\omega_v = 18.9$ r/s

Initial Values

$F(o) = 0$
$H = 0$
$K_p = 1.0$
$m_v^* = 1068$
$\Delta m_v(o) = 0$
$\Delta \dot{m}_v(o) = 0$
$N(o) = 0$
$P(o) = 0$

$P_B(o) = F$
$z_a(o) = 0$
$\dot{z}_a(o) = 0$
$z_g(o) = 0$
$\dot{z}_g(o) = 0$
$\delta(o) = 0.42$
$\delta_d^*(o) = 0.42$

APPENDIX B

Cushion Volume Equations

The cushion volume is given by

$$V = V_F + V_\perp$$

where

$$V_F = C_\perp + C_2 B_0 + C_3 H$$

$$V_{\perp} = \begin{cases} V_{\perp a}, & 0 \leq z < z_{\perp} \\ V_{\perp b}, & z_{\perp} \leq z < z_2 \\ V_{\perp c}, & z_2 \leq z \end{cases}$$

$$V_{\perp a} = B_0 z + C_4 z^2$$

$$V_{\perp b} = C_5 + C_6 z + C_7 z^2$$

$$V_{\perp c} = C_8 + B_2 z$$

and

$$C_4 = 0.5\ (B_{\perp} - B_0)/z_{\perp}$$

$$C_5 = 0.5 z_{\perp}(\alpha z_{\perp} + B_0 - B_{\perp})$$

$$C_6 = B_{\perp} - \alpha z_{\perp}$$

$$C_7 = \alpha/2$$

$$C_8 = C_5 + (C_6 - B_2) z_2 + C_7 z_2^2$$

and

$$B_0 = k_a B_{0n}$$

$$B_{\perp} = k_a B_{\perp n}$$

$$B_2 = k_a B_{2n}$$

$$\alpha = (B_2 - B_{\perp})/(z_2 - z_{\perp})$$